Insights into mechanisms for reductive dechlorination by sulfidated nanoscale zerovalent iron

Congyu Gao

Degree of Master of Science

Department of Civil Engineering

McGill University, Montreal

A thesis submitted to the Graduate and Postdoctoral Studies Office in partial fulfilment of the requirements of the degree of Master of Science

July 2023

Abstract

Sulfidation of nanoscale zerovalent iron (nZVI) results in nanoparticles that are a composite of iron sulfides, iron oxides and Fe(0), and are significantly more reactive and colloidally stable than nZVI alone. Sulfidated nZVI (S-nZVI) possesses high reactivity towards several chlorinated aliphatic hydrocarbons and yet has reduced reactivity to water , which provides higher selectivity to target chlorinated aliphatic hydrocarbons in aqueous matrices. The rates and extents of target compound degradation by S-nZVI is known to be influenced by the S and Fe precursors, the synthesis procedure (one-pot or two-pot procedure) the sulfur content of the S-nZVI and pollutant type. The limited anaerobic corrosion with water is attributable to the surface hydrophobicity of iron sulfides, but the active sites responsible for high reactivity to pollutants such as trichloroethene and carbon tetrachloride has not been clearly elucidated. The objective of this study was to improve the understanding of why nZVI sulfidation extent affects the reactivity of S-nZVI to carbon tetrachloride and trichloroethene. Based on previous studies in our laboratory, the co-precipitated S-nZVI synthesized using Na_2S, which provided the highest reactivity to trichloroethene was selected for investigation. Solvent kinetic isotope effect (SKIE) assays were carried out and the results indicate that atomic hydrogen does not contribute to high reactivity to the target compounds. A series of experiments were conducted where S-nZVI with different sulfidation extents were reacted with phosphate, a chemical species that competes with the target contaminants with some of the active sites on S-nZVI. The results conclusively demonstrates that direct electron transfer at iron (hydr)oxides sites contribute to high reactivity to contaminants such as carbon tetrachloride, whereas electron transfer at FeS sites contribute to high reactivity to trichloroethene. The results suggest that morphological changes arising from

particle break-up also contribute to the formation of new reactive sites which result in high particle reactivity.

A comprehensive literature review of different proposed mechanisms is provided in the first chapter. The following chapter describes batch experiments to investigate the role of atomic hydrogen (reactive hydrogen species) towards the reactivity of S-nZVI to chlorinated solvent compounds, using the solvent kinetic isotope effect method. The third chapter describes experimental methods and results on the effect of presence of a competing anion on the reactivity of S-nZVI towards investigation of active sites for reactivity of chlorinated solvent compounds. The final chapter summarizes and discusses the significance of the findings in Chapters 2 and 3.

Keywords: S-nZVI, site remediation, reductive dechlorination, atomic hydrogen, active site, Langmuir-Hinshelwood-Hougen-Watson (LHHW) model.

Résumé

La sulfuration du fer zéro-valent à l'échelle nanométrique (nZVI) conduit à des nanoparticules composées de FeS et de Fe(0) et qui sont significativement plus réactives et colloidales que le nZVI seul. Le nZVI sulfaté (S-nZVI) présente une grande réactivité envers plusieurs hydrocarbures aliphatiques chlorés et pourtant, il a une faible vitesse d'évolution de l'hydrogène, ce qui confère une grande sélectivité aux hydrocarbures aliphatiques chlorés cibles dans les matrices aqueuses. Les taux et les étendues de dégradation des composés cibles par le S-nZVI sont connus pour être influencés par les précurseurs de soufre et de fer, la procédure de synthèse (procédure en une étape ou en deux étapes), la teneur en soufre du S-nZVI et le type de polluant. La corrosion anaérobie limitée avec l'eau est attribuable à l'hydrophobicité de surface du sulfure de fer, mais les sites actifs responsables de la grande réactivité envers les polluants tels que le trichloroéthène et le tétrachlorure de carbone n'ont pas été clairement élucidés. L'objectif de cette étude était d'améliorer la compréhension de pourquoi l'étendue de la sulfuration du nZVI affecte la réactivité du S-nZVI envers le tétrachlorure de carbone et le trichloroéthylène. Sur la base d'études antérieures menées dans notre laboratoire, le S-nZVI coprécipité synthétisé à l'aide de Na2S, qui a montré la plus grande réactivité envers le trichloroéthène, a été sélectionné pour l'investigation. Des essais d'effet isotopique cinétique du solvant (SKIE) ont été réalisés, et les résultats indiquent que l'hydrogène atomique ne contribue pas à la grande réactivité envers les composés cibles. Une série d'expériences a été menée où des S-nZVI avec différentes étendues de sulfuration ont été mis en réaction avec du phosphate, une espèce chimique qui compétitionne avec les contaminants cibles pour certains des sites actifs sur le S-nZVI. Les résultats démontrent de manière concluante que le transfert d'électrons direct aux sites d'oxyde de fer contribue à la

grande réactivité envers les contaminants tels que le tétrachlorure de carbone, tandis que le transfert d'électrons aux sites de FeS contribue à la grande réactivité envers le trichloroéthène. Les résultats suggèrent que les changements morphologiques résultant de la fragmentation des particules contribuent également à la formation de nouveaux sites réactifs, ce qui entraîne une grande réactivité des particules.

Une revue exhaustive de la littérature sur les différents mécanismes proposés par différents groupes est fournie dans le premier chapitre. Le chapitre suivant décrit des expériences en lot pour étudier le rôle de l'hydrogène atomique (espèces d'hydrogène réactives) dans la réactivité du S-nZVI envers les composés solvants chlorés, en utilisant la méthode de l'effet isotopique cinétique du solvant. Le dernier chapitre décrit les méthodes expérimentales et les résultats sur l'effet de la présence d'un anion concurrent sur la réactivité du S-nZVI dans le cadre de l'étude des sites actifs pour la réactivité des composés solvants chlorés.

Acknowledgments

I would like to express my sincere gratitude to my supervisor Prof. Subhasis Ghoshal, whose guidance and support throughout this research project has been invaluable. Their insightful comments, constructive criticism and encouragement have been instrumental in shaping my work.

I am also grateful to the faculty members of Civil Engineering, for their encouragement, assistance and support in various aspects of my academic pursuits.

My heartfelt appreciation goes to my family, for their unwavering support, love and encouragement throughout my studies. Without their constant motivation, this achievement would not have been possible.

Lastly, I would like to express my gratitude to my colleagues in the Environmental Engineering Laboratory who helped me during my study.

Thank you all for your support and encouragement.

Table of Content

Abstract 2

Résumé 4

Acknowledgments 6

Chapter 1 Literature Review 9

1.1 Background of Site Remediation 9

1.1.1 Chlorinated Solvent Contamination of the Subsurface and its Remediation 9

1.2 Nanotechnology and Their Potential for Groundwater Remediation 11

1.2.1 Nano-scale Zero Valent Iron (nZVI) for Groundwater Remediation 12

1.3 Sulfidated Nano-scale Zero Valent Iron (S-nZVI): A More Reactive Version of S-nZVI 13

Reference 17

Chapter 2 Assessing the Generation of Atomic Hydrogen Species by Sulfidated nZVI 26

2.1 Introduction 26

2.2 Methods and Materials 28

2.2.1 Chemicals 28

2.2.2 Synthesis 28

2.2.3 Reactivity Experiments 30

2.2.4 Hydrogen Uptake Experiment 31

2.2.5 Analytical Methods 31

2.3 Results and Discussion 32

2.3.1 SKIE experiment with S-nZVI of TCE and CT 32

2.3.2 Hydrogen uptake experiment with Pd-nZVI and S-nZVI with TCE 34

Reference 37

Chapter 3 Investigation of Active Sites in S-nZVI responsible for degradation of different chlorinated solvent compounds 39

3.1 Introduction 39

3.2 Methods and Materials 42
3.2.1 Chemicals 42
3.2.2 Synthesis 42
3.2.3 Batch Experiments 42
3.2.4 Analytical Method 43
3.2.5 Kinetic Model 43
3.3 Result and Discussion 45
3.3.1 Phosphate Ion Competition Experiments for S-nZVI with for Different Sulfur Doses and CHCs 45
3.3.2 An Active Site Mechanism Revealed by Phosphate Ion Competition Experiment 48
3.3.3 Inter-species Competition Experiment of S-nZVI between CT and TCE 52
Supplementary Information 61
Reference 73
Chapter 4. Overall Conclusions and Discussion 79
4.1 Major Conclusions 79
4.2 Limitations 81
Reference 82

Chapter 1 Literature Review

1.1 Background of Site Remediation

Previously, toxic liquid wastes were disposed of in ways that disregarded the possibility that they would linger in the subsurface for a very long time and perhaps pollute drinking water supplies. The disposal techniques used included surface spills, leaky storage ponds, and direct dumping of the liquid waste into the earth. The inappropriate disposal of waste liquids from industrial operations as non-aqueous phase liquids (NAPLs), such as oils, solvents, and tars with significant toxic chemical concentrations, have resulted in long-term pollution. Brownfields and industrialized sites frequently include and chlorinated solvents, which are particularly tenacious NAPL pollutants that can poison water supplies for many years.

The difficulties posed by polluted sites have underlined the need to create remediation methods that can be applied in a range of physical situations and are both practical and efficient. The general public, the government, and business are now aware of the potential threats that toxic chemical mixtures bring to the environment and to human health. Hence, several remediation strategies, including steam and density adjusted displacement of NAPLs, stabilization/solidification, and in situ redox chemical processes, have been developed to remediate NAPL-contaminated sites[1-4].

1.1.1 Chlorinated Solvent Contamination of the Subsurface and its Remediation

Chlorinated solvents are widely used as reagents and as degreasing solvents in the manufacturing industry [44]. Given the large volumes that are used, accidental spills and improper storage and

disposal methods employed in the past, have led to large volumes of chlorinated solvent contamination in the subsurface. When discharged into soil, the fate and transport of chlorinated solvents is affected by a variety of physical, chemical, and hydrogeological properties of the site[44, 45]. The solvent may be able to travel deeper into the subsurface owing to gravity through porous soil layers which comprise the vadose zone. The vadose zone lies between the ground surface and the groundwater table, is primarily made up of moisture, air or gases in between soil particles. As the solvent phase migrates through this layer it will leave some solvent in the soil as residual saturation. If enough solvent is leaked, it may ultimately get into the groundwater. Most chlorinated solvents are denser than water, and thus can penetrate the groundwater saturated soil layers to reach deeper layers or the bed rock of aquifers. The solvent may pool on top of or find a way around clay layers when it encounters them. This complex distribution of chlorinated solvents in the subsurface makes its extraction difficult, and these solvent pools contribute to extensive groundwater plumes which can be sustained by the slow but continuous release of the contaminants.

The chlorinated solvents dissolve into the groundwater when it passes through porous strata, resulting in the formation of a polluted groundwater plume[46, 47]. This plume may reach a well that provides groundwater to people on the surface and contaminate it, or it could exit and enter a stream or other open water source. Addressing both the dense nonaqueous phase liquids (DNAPL) source and the polluted plume is necessary for the cleanup of a site contaminated by a chlorinated solvent. To address these issues, a number of methods have been created, including pump-and-treat[47], air-injection systems[48], and surfactant flushing[49]. These technologies rely on flushing water, air, or solubilizing chemicals, which are captured by collection well, and the contaminated water or air stream is then treated above ground. In addition, bioremediation is also

a very promising strategy. Numerous categories of bacteria, such as *Dehalococcoides* spp., *Dehalobacter* spp., possess the capability to perform dehalogenation of chlorinated aliphatic and aromatic hydrocarbons in anaerobic environments[50-53].

1.2 Nanotechnology and Their Potential for Groundwater Remediation

Advanced nanomaterials that can enhance in situ cleanup of pervasive and persistent pollutants, are now possible because to recent developments in materials science and nanotechnology. The ability of multifunctional nanomaterials to target numerous pollutants at once and demonstrate stronger selectivity towards contaminants than other matrix components has changed the design and synthesis of materials for in situ cleanup[5]. Moreover, using engineered nanoparticles with adaptable surface functions might help define the parameters of the subsurface environment and provide information[6-8].

Additionally, the effectiveness of sequestration/degradation of targeted contaminants can be increased by using composite nanomaterials that can adapt to changes in the environment and respond to geochemical stimulants such as pH, temperature, or redox changes[9-11].

Nanotechnology, exemplified by the utilization of materials such TiO_2 nanoparticles and nanoscale zerovalent iron, finds extensive practical applications in the real-world context for water treatment. TiO_2 nanoparticles[12], produce reactive oxidants such as OH radicals under exposure to light, to for contaminant degradation. TiO_2-based films and membranes also provide organic pollutant decomposition Due to their relatively high cost and photoactivation needs, TiO_2 nanoparticles are generally used for *ex situ* treatment of contaminated groundwaters. Nanoscale zero valent iron (nZVI)[5], due to their spontaneous ability to give up electrons in corrosion

reactions with water, and relatively low cost and toxicity, are preferred for in situ groundwater remediation operations of chlorinated solvent compounds (and other highly oxidized contaminants), nitrates, and metal pollutants.

1.2.1 Nano-scale Zero Valent Iron (nZVI) for Groundwater Remediation

Engineered nanomaterial needs to be non-toxic, earth-abundant and cost-effective, which makes nanoscale zero valent iron (nZVI) widely accepted for groundwater remediation[13] for decades. Due to their unique characteristics, iron nanoparticles have become a viable technique for nano-remediation. These particles have a typical core shell structure and are typically synthesized in the laboratory from Fe (II) and Fe (III) salt solution using borohydride as the reductant. The metallic iron in the core of these particles undergoes oxidation by water, even under anoxic conditions, to produce mixed valent [Fe (II) and Fe (III)] oxide in the shells, which then stabilizes the Fe(0) core from further rapid oxidation. The nanoscale zerovalent iron particles have higher reactivity over micro-sized ones because they have a larger surface area[14] and more reactive sites that make it possible for them to render a variety of pollutants, such as carbon tetrachloride (CT), trichloroethylene (TCE) and tetrachloroethene (PCE). For example, Singh et al.[17] found that nZVI can degrade a pesticide called Endosulfan 300 times faster than micro-scale zero valent iron (mZVI) partly due to its much higher specific surface area (i.e., nZVI – 33.21 m^2g^{-1}; mZVI – 0.43 m^2g^{-1}).

To increase efficiency of reactivity with target pollutants, zero valent iron can also be functionalized with coatings of polyelectrolytes or polymers to improve colloidal stability[15]. For example, polyacrylic acid (PAA) has been used for polymer-coating of nZVI[54], which resulted in

improved mobility in carbonate porous media by generating potent repulsive interactions between PAA/nZVI and the carbonate matrix. Other coatings with catalysts, such as palladium[16], can also improve the particle reactivity by generating atomic hydrogen. Xie and Ciwertny[55] reported a 10-fold increase in 1,1,1,2-tetrachloroethane degradation kinetics by Pd-nZVI compared to nZVI, which was attributed to the generation of atomic hydrogen by the doped Pd.

TCE is a common and toxic chlorinated pollutant in groundwater, may be removed effectively by using a bimetallic nanocomposite called palladium-doped[18] nanoscale zero valent iron (Pd-nZVI), which catalyzes the oxidation-reduction process. Vinyl chloride and other chlorinated intermediates, which are frequently produced during anaerobic bioremediation and with bulk iron metal, were found to be nonexistent in significant quantities when TCE was converted into ethane using Pd-nZVI[19,20].

1.3 Sulfidated Nano-scale Zero Valent Iron (S-nZVI): A More Reactive Version of S-nZVI

Kim et al.[22] first reported that the addition of dithionite ($Na_2S_2O_4$) during the borohydride reduction of ferric chloride resulted in the production of 'Fe/FeS' nanoparticles. Such a nanocomposites made of iron and iron sulfides had higher reactivity toward TCE than nZVI synthesized without the addition of dithionite. Since then, the literature on the effectiveness of sulfur-induced enhancement in reactivity of nZVI in the removal of contaminants, such as metals and metalloids, organic dyes, pharmaceuticals, and chlorinated hydrocarbons such as TCE, under both aerobic and anaerobic conditions, has increased significantly.

For the synthesis of sulfidized nanoscale zerovalent iron (S-nZVI), a number of sulfidation techniques have been suggested[23,31,39,56-58]. An aqueous solution of Fe^{2+} or Fe^{3+} is added

dropwise to a sulfur precursor (e.g., $Na_2S_2O_4$ or Na_2S) and $NaBH_4$ solution in a co-precipitation method. An alternative technique (post-sulfidation) uses Na_2S or other sulfur precursors to sulfidize already-formed nZVI particles. These techniques provide flexibility in adjusting S-nZVI properties for different applications. For the co-precipitation method, also called one-step synthesis, sulfur is uniformly distributed in S-nZVI particles[5]. Post-sulfidation, on the other hand, deposits sulfur species on pre-synthesized nZVI and involves a two-step synthesis[32]. Several studies have outlined how the electrical conductivity, hydrophobicity, and sulfur distribution (i.e., core and shell) of S-nZVI vary depending on the sulfidation process and the molar ratio of S to Fe supplied during synthesis[30,40].

The integration of sulfur into nZVI produces a significant influence on the rates and extents of dechlorination of TCE. For more than one decade, researchers have carried out in-depth work to find out the mechanism behind S-nZVI and yet this topic remains controversial due to a lack of direct proof for the mechanisms cited. Several mechanisms presented in the literature are described below.

Kim et al.[22] suggested that the iron sulfides shell acts as a bridge to transfer electrons from the iron core to the surface and these electrons are directly accessible to reduce adsorbed pollutant molecules (e.g., trichloroethene). EFM (electrostatic force microscopy) images show a much higher brightness by S-nZVI than nZVI, as well as a higher R_{rms} (EFM roughness value), suggesting the incorporated sulfur facilitates the electron flow.

Rajajayavel et al.[23] showed that the sulfidation in nanoscale zerovalent iron (nZVI) accelerates the rate of trichloroethylene (TCE) dechlorination, with a surface-area normalized first-order degradation rate constant increasing up to 40 times that of non-sulfidated nZVI. They attributed this enhancement to the fact that sulfidated nZVI inhibited corrosion processes in water and 33%

less electron was consumed. As a result, more electrons were available for target pollutant removal.

Beyond that, Han and Yan[24] argued that atomic hydrogen, is formed on the iron sulfides and trichloroethene is mainly reduced by atomic hydrogen on iron surface, according to the electrochemistry measurement[43]. They observed enhanced TCE degradation by S-nZVI than nZVI but did not observe same trend for carbon tetrachloride (CT). Since TCE degradation is facilitated by atomic hydrogen while CT degradation results from direct electron transfer, they suggested that the iron sulfides functions as the site that poisons the recombination of atomic hydrogen to form hydrogen gas. This theory was opposed by Cao et al.[41] that they observed no impact of S-nZVI reactivity in the presence of tert-butanol (TBA), which is a scavenger for atomic hydrogen and hydroxyl radical. One most recent theory by Mangayayam et al.[42] argued how the amount of inactive $Fe(OH)_2$ sites lower the accessibility of pollutant to the active sites comprised of Fe(0) and FeS present on S-nZVI surface controlled the degradation trend of TCE and cis-DCE with different sulfur doses, but no follow-up experimental proof were provided. Although these theories explains specific experiment results with single pollutants or those with similar structure, the extrapolation to others is impossible because these theories are somewhat contradictory to each other, which leads to a major knowledge gap.

Moreover, Xu et al.[40] synthesized S-nZVI with $Na_2S_2O_4$ and $FeCl_3$ showed very strong hydrophobicity. It showed a very low hydrogen evolution rate, i.e., reaction with water compared to other more hydrophilic S-nZVI and the highest TCE degradation rate. So, the hydrophobicity could also play a role as it inhibits the side reaction that competes for electrons and make the surface more accessible to hydrophobic molecules. However, hydrophobicity alone cannot explain the enhanced dechlorination efficiency because not all hydrophobic molecules can be

degraded rapidly by S-nZVI. The octanol partition coefficient (K_{ow}), a measure of hydrophobicity of a compound, for carbon tetrachloride (CT) and trichloroethylene (TCE) provides a typical counterexample. It is noteworthy that their degradation rate constants show a significant disparity, exceeding a 100-fold difference[21], despite the remarkable similarity in their respective partition coefficient values.

The advantages that nZVI provides through controlled sulfidation, such as increased reactivity in transforming contaminants[22-24], improved contaminant sequestration[25-27], better selectivity, longevity, and reduced aggregation[28-29], makes it an efficient option for remediation than nZVI, and more cost-effective remediation agent than Pd-nZVI.

Reference

[1] Fruchter, J. S., Cole, C., Williams, M., Vermeul, V. R., Amonette, J. E., Szecsody, J. E., Istok, J. D., & Humphrey, M. D. (2000). Creation of a Subsurface Permeable Treatment Zone for Aqueous Chromate Contamination Using In Situ Redox Manipulation. Ground Water Monitoring and Remediation, 20(2), 66–77.

[2] Ramsburg, C. A., & Pennell, K. D. (2002). Density-Modified Displacement for DNAPL Source zone remediation: density conversion and recovery in heterogeneous aquifer cells. Environmental Science & Technology, 36(14), 3176–3187.

[3] She, H. Y., & Sleep, B. E. (1999). Removal of Perchloroethylene from a Layered Soil System by Steam Flushing. Ground Water Monitoring and Remediation, 19(2), 70–77.

[4] USEPA. Solidification/stabilization use at superfund sites. Cinnacinati, OH: United States Environmental Protection Agency; 2000. EPA-542-R-00-010.

[5] Bhattacharjee, S., & Ghoshal, S. (2018). Optimal design of sulfidated nanoscale zerovalent iron for enhanced trichloroethene degradation. Environmental Science & Technology, 52(19), 11078–11086.

[6] Hwang, C., Ruan, G., Wang, L., Zheng, H., Samuel, E. L. G., Xiang, C., Lu, W., Kasper, W., Huang, K., Peng, Z., Schaefer, Z. L., Kan, A. T., Martí, Á. A., Wong, M. S., Tomson, M. B., & Tour, J. M. (2014). Carbon-Based nanoreporters designed for subsurface hydrogen sulfide detection. ACS Applied Materials & Interfaces, 6(10), 7652–7658.

[7] Berlin, J. M., Yu, J., Lu, W., Walsh, E. E., Zhang, L., Zhang, P., Chen, W., Kan, A. T., Wong, M. S., Tomson, M. B., & Tour, J. M. (2011). Engineered nanoparticles for hydrocarbon detection in oil-field rocks. Energy and Environmental Science, 4(2), 505–509.

[8] Hwang, C., Wang, L., Lu, W., Ruan, G., Kini, G. C., Xiang, C., Samuel, E. L. G., Shi, W., Kan, A. T., Wong, M. S., Tomson, M. B., & Tour, J. M. (2012). Highly stable carbon nanoparticles designed for downhole hydrocarbon detection. Energy and Environmental Science, 5(8), 8304.

[9] Burello, E. (2015). Computational design of safer nanomaterials. Environmental Science. Nano, 2(5), 454–462.

[10] Chen, P. C., Liu, X., Hedrick, J. L., Xie, Z., Wang, S., Lin, Q., Hersam, M. C., Dravid, V. P., & Mirkin, C. A. (2016). Polyelemental nanoparticle libraries. Science, 352(6293), 1565–1569.

[11] Vyatskikh, A., Delalande, S., Kudo, A. et al. Additive manufacturing of 3D nano-architected metals. Nat Commun 9, 593 (2018).

[12] Amin, M., Alazba, A. A., & Manzoor, U. (2014). A Review of Removal of Pollutants from Water/Wastewater Using Different Types of Nanomaterials. Advances in Materials Science and Engineering, 2014, 1–24.

[13] Nadagouda, M. N., & Varma, R. S. (2009). Risk Reduction Via Greener Synthesis of Noble Metal Nanostructures and Nanocomposites. In NATO science for peace and security series (pp. 209–217).

[14] Tratnyek, P. G., & Johnson, R. L. (2006). Nanotechnologies for environmental cleanup. Nano Today, 1(2), 44–48.

[15] Navid Saleh, Kevin Sirk, Yueqiang Liu, Tanapon Phenrat, Bruno Dufour, Krzysztof Matyjaszewski, Robert D. Tilton, and Gregory V. Lowry. Surface Modifications Enhance Nanoiron Transport and NAPL Targeting in Saturated Porous Media. Environmental Engineering Science.Jan 2007.45-57.

[16] Bhattacharjee, S., Basnet, M., Tufenkji, N., & Ghoshal, S. (2016). Effects of rhamnolipid and carboxymethylcellulose coatings on reactivity of Palladium-Doped nanoscale zerovalent iron particles. Environmental Science & Technology, 50(4), 1812–1820.

[17] Singh, S. P., & Bose, P. (2015). Degradation kinetics of Endosulfan isomers by micron- and nano-sized zero valent iron particles (MZVI and NZVI). Journal of Chemical Technology & Biotechnology, 91(8), 2313–2321.

[18] Otto, M., Floyd, M., & Bajpai, S. (2008). Nanotechnology for site remediation. Remediation Journal, 19(1), 99–108.

[19] Nutt, M. O., Heck, K. N., Alvarez, P. J. J., & Wong, M. S. (2006). Improved Pd-on-Au bimetallic nanoparticle catalysts for aqueous-phase trichloroethene hydrodechlorination. Applied Catalysis B-Environmental, 69(1–2), 115–125.

[20] Bhattacharjee, S., & Ghoshal, S. (2016). Phase transfer of palladized nanoscale zerovalent iron for environmental remediation of trichloroethene. Environmental Science & Technology, 50(16), 8631–8639.

[21] Zhang, Y., Ozcer, P. O., & Ghoshal, S. (2021). A comprehensive assessment of the degradation of C1 and C2 chlorinated hydrocarbons by sulfidated nanoscale zerovalent iron. Water Research, 201, 117328.

[22] Kim, E., Kim, J., Azad, A., & Chang, Y. S. (2011). Facile synthesis and characterization of FE/FES nanoparticles for environmental applications. ACS Applied Materials & Interfaces, 3(5), 1457–1462.

[23] Rajajayavel, S. R. C., & Ghoshal, S. (2015). Enhanced reductive dechlorination of trichloroethylene by sulfidated nanoscale zerovalent iron. Water Research, 78, 144–153.

[24] Han, Y., & Yan, W. (2016). Reductive Dechlorination of Trichloroethene by Zero-valent Iron Nanoparticles: Reactivity Enhancement through Sulfidation Treatment. Environmental Science & Technology, 50(23), 12992–13001.

[25] Fan, D., Anitori, R., Tebo, B. M., Tratnyek, P. G., Pacheco, J. S. L., Kukkadapu, R., Engelhard, M. H., Bowden, M. E., Kovařík, L., & Arey, B. W. (2013). Reductive Sequestration of Pertechnetate (99TcO4–) by Nano Zerovalent Iron (nZVI) Transformed by Abiotic Sulfide. Environmental Science & Technology, 47(10), 5302–5310.

[26] Su, Y., Adeleye, A. S., Keller, A. A., Huang, Y., Dai, C., Zhou, X., & Zhang, Y. (2015). Magnetic sulfide-modified nanoscale zerovalent iron (S-nZVI) for dissolved metal ion removal. Water Research, 74, 47–57.

[27] Du, J., Bao, J., Lu, C., & Werner, D. (2016). Reductive sequestration of chromate by hierarchical FeS@Fe0 particles. Water Research, 102, 73–81.

[28] Fan, D., Johnson, G. O., Tratnyek, P. G., & Johnson, R. L. (2016). Sulfidation of nano zerovalent iron (NZVI) for improved selectivity during In-Situ Chemical Reduction (ISCR). Environmental Science & Technology, 50(17), 9558–9565.

[29] Song, S., Su, Y., Adeleye, A. S., Zhang, Y., & Zhou, X. (2017). Optimal design and characterization of sulfide-modified nanoscale zerovalent iron for diclofenac removal. Applied Catalysis B-Environmental, 201, 211–220.

[30] Xu, J., Avellan, A., Li, H., Liu, X., Noël, V., Lou, Z., Wu, Y., Kaegi, R., Henkelman, G., & Lowry, G. V. (2020). Sulfur loading and speciation control the hydrophobicity, electron transfer, reactivity, and selectivity of sulfidized nanoscale zerovalent iron. Advanced Materials, 32(17), 1906910.

[31] Lv, D., Zhou, J., Cao, Z., Xu, J., Liu, Y., Li, Y., Yang, K., Lou, Z., Lou, L., & Xu, X. (2019). Mechanism and influence factors of chromium(VI) removal by sulfide-modified nanoscale zerovalent iron. Chemosphere, 224, 306–315.

[32] Li, J., Zhang, X., Sun, Y., Liang, L., Pan, B., Zhang, W., & Guan, X. (2017). Advances in sulfidation of zerovalent iron for water decontamination. Environmental Science & Technology, 51(23), 13533–13544.

[33] Hoch, L., Mack, E. J., Hydutsky, B. W., Hershman, J. M., Skluzacek, J. M., & Mallouk, T. E. (2008). Carbothermal synthesis of carbon-supported nanoscale zero-valent iron particles for the remediation of hexavalent chromium. Environmental Science & Technology, 42(7), 2600–2605.

[34] Bystrzejewski, M. (2011). Synthesis of carbon-encapsulated iron nanoparticles via solid state reduction of iron oxide nanoparticles. Journal of Solid State Chemistry, 184(6), 1492–1498.

[35] Tao, N., Sui, M., Lü, J., & Lua, K. (1999). Surface nanocrystallization of iron induced by ultrasonic shot peening. Nanostructured Materials, 11(4), 433–440.

[36] Chen, S., Hsu, H., & Li, C. (2004). A new method to produce nanoscale iron for nitrate removal. Journal of Nanoparticle Research, 6(6), 639–647.

[37] Yoo, B., Hernández, S. C., Koo, B. K., Rheem, Y., & Myung, N. V. (2007). Electrochemically fabricated zero-valent iron, iron-nickel, and iron-palladium nanowires for environmental remediation applications. Water Science and Technology, 55(1–2), 149–156.

[38] Hoag, G. E., Collins, J. B., Holcomb, J., Hoag, J. R., Nadagouda, M. N., & Varma, R. S. (2009). Degradation of bromothymol blue by 'greener' nano-scale zero-valent iron synthesized using tea polyphenols. Journal of Materials Chemistry, 19(45), 8671.

[39] Duan, J., Ji, H., Liu, W., Zhao, X., Han, B., Tian, S., & Zhao, D. (2019). Enhanced immobilization of U(VI) using a new type of FeS-modified Fe0 core-shell particles. Chemical Engineering Journal, 359, 1617–1628.

[40] Xu, J., Avellan, A., Li, H., Clark, E. A., Henkelman, G., Kaegi, R., & Lowry, G. V. (2020). Iron and sulfur precursors affect crystalline structure, speciation, and reactivity of sulfidized nanoscale zerovalent iron. Environmental Science & Technology, 54(20), 13294–13303.

[41] Cao, Z., Li, H., Lowry, G. V., Shi, X., Pan, X., Xu, X., Henkelman, G., & Xu, J. (2021). Unveiling the Role of Sulfur in Rapid Defluorination of Florfenicol by Sulfidized Nanoscale Zero-Valent Iron in Water under Ambient Conditions. Environmental Science & Technology, 55(4), 2628–2638.

[42] Mangayayam, M. C., Dideriksen, K., Ceccato, M., & Tobler, D. J. (2019). The structure of sulfidized Zero-Valent iron by One-Pot Synthesis: Impact on contaminant selectivity and Long-Term performance. Environmental Science & Technology, 53(8), 4389–4396.

[43] Li, T., & Farrell, J. (2001). Electrochemical Investigation of the Rate-Limiting Mechanisms for trichloroethylene and carbon tetrachloride reduction at iron surfaces. Environmental Science & Technology, 35(17), 3560–3565.

[44] McCarty, P. L. (2010). Groundwater contamination by chlorinated solvents: history, remediation technologies and strategies. In SERDP and ESTCP remediation technology monograph serie (pp. 1–28).

[45] Wiedemeier, T. H., Rifai, H. S., Newell, C. J., & Wilson, J. T. (1999). Natural attenuation of fuels and chlorinated solvents in the subsurface. In John Wiley & Sons, Inc. eBooks.

[46] Rivett, M. O., Feenstra, S., & Cherry, J. A. (2001). A controlled field experiment on groundwater contamination by a multicomponent DNAPL: creation of the emplaced-source and overview of dissolved plume development. Journal of Contaminant Hydrology, 49(1–2), 111–149.

[47] Lawrence, A., Stuart, M., Barker, J. A., & Tester, D. J. (1996). Contamination of chalk groundwater by chlorinated solvents: A case study of deep penetration by Non-Aqueous Phase Liquids. Water and Environment Journal, 10(4), 263–272.

[48] Nyer, E. K., Palmer, P. L., Carman, E. P., Boettcher, G., Bedessem, J. M., Lenzo, F., Crossman, T. L., Rorech, G. J., & Kidd, D. F. (2001). In Situ Treatment Technology (2nd ed.). CRC Press.

[49] Mulligan, C. N., Yong, R. N., & Gibbs, B. F. (2001). Surfactant-enhanced remediation of contaminated soil: a review. Engineering Geology, 60(1–4), 371–380.

[50] Kranzioch, I., Stoll, C., Holbach, A., Chen, H., Wang, L., Zheng, B., Norra, S., Bi, Y., Schramm, K., & Tiehm, A. (2013). Dechlorination and organohalide-respiring bacteria dynamics in sediment samples of the Yangtze Three Gorges Reservoir. Environmental Science and Pollution Research, 20(10), 7046–7056.

[51] Field, J. A., & Sierra-Álvarez, R. (2007). Microbial degradation of chlorinated benzenes. Biodegradation, 19(4), 463–480.

[52] Taş, N., Van Eekert, M., Wagner, A., Schraa, G., De Vos, W. M., & Smidt, H. (2011). Role of "Dehalococcoides" spp. in the Anaerobic Transformation of Hexachlorobenzene in European Rivers. Applied and Environmental Microbiology, 77(13), 4437–4445.

[53] Bedard, D. L. (2008). A case study for microbial biodegradation: Anaerobic bacterial Reductive dechlorination of Polychlorinated Biphenyls—From Sediment to Defined Medium. Annual Review of Microbiology, 62(1), 253–270.

[54] Laumann, S., Micić, V., & Hofmann, T. (2014). Mobility enhancement of nanoscale zero-valent iron in carbonate porous media through co-injection of polyelectrolytes. Water Research, 50, 70–79.

[55] Xie, Y., & Cwiertny, D. M. (2013). Chlorinated Solvent Transformation by Palladized Zerovalent Iron: Mechanistic Insights from Reductant Loading Studies and Solvent Kinetic Isotope Effects. Environmental Science & Technology, 47(14), 7940–7948.

[56] Wang, B., Dong, H., Li, L., Wang, Y., Qin, N., Tang, L., & Zeng, G. (2020). Influence of different co-contaminants on trichloroethylene removal by sulfide-modified nanoscale zero-valent iron. Chemical Engineering Journal, 381, 122773.

[57] Rayaroth, M. P., Prasanthkumar, K. P., Kang, Y., Lee, C., & Chang, Y. S. (2020). Degradation of carbamazepine by singlet oxygen from sulfidized nanoscale zero-valent iron – citric acid system. Chemical Engineering Journal, 382, 122828.

[58] Miao, L., Zhao, J., Hou, J., Zeng, R. J., & Xing, B. (2019). Degradation of Tetrabromobisphenol A by Sulfidated Nanoscale Zerovalent Iron in a Dynamic Two-Step Anoxic/Oxic Process. Environmental Science & Technology, 53(14), 8105–8114.

Chapter 2 Assessing the Generation of Atomic Hydrogen Species by Sulfidated nZVI

2.1 Introduction

Isotopic substitution is a promising approach that has been used to investigate reaction mechanisms. This method involves comparing reaction kinetics between isotope-labelled and non-labelled compounds without significantly altering the structural makeup of the system. The effectiveness of isotopic substitution can be attributed to the fact that all isotope effects ultimately depend on the relative masses of the labelled and unlabelled nuclei involved. Hydrogen isotopes have the highest ratio of masses, making them ideal for comparison studies. As a result, a large number of studies have been conducted comparing deuterium-containing substrates with their protium-containing counterparts[1-4].

Solvent kinetic isotope effects (SKIEs) may be observed when an isotopically substituted version of the solvent is used if it functions as a reactant or if it interacts strongly with the transition structures that are created during the reaction. For reactions involving water, an approach that has been used in previous studies is assessing the impacts on reaction rates by switching the solvent from H_2O to D_2O. Xie and Ciwertny[5] measured SKIEs for specific reductants and system variables in order to investigate the circumstances that favor the involvement of atomic hydrogen in the reduction of chlorinated solvents (i.e., 1,1,1,2-tetrachloroethane (1,1,1,2-TeCA) and cis-dichloroethene (DCE)) in aqueous media using palladium-doped nanoscale zero valent iron (Pd-nZVI). Larger SKIEs (i.e., rate constant ratio in H_2O and D_2O: $k_H/k_D \sim 20$) was taken as

evidence that atomic hydrogen generated from the reduction of water was contributing to the transformation of organohalides.

As discussed in the previous chapter, there are proposed reaction mechanisms for chlorinated solvent compound degradation[6-7] that suggest the involvement of atomic hydrogen generated from S-nZVI particles, either on iron sulfides site or iron (hydr)oxides sites, upon reaction with water. Han and Yan[6], argued that a decrease in hydrogen evolution rate and a similar level of enhancement in TCE degradation by S-nZVI and As-doped nZVI suggested the generation of atomic hydrogen. However, the observed suppression of hydrogen evolution could be attributed to the hydrophobic or low water affinity nature of iron sulfide. Additionally, arsenic exhibits markedly different chemical properties than sulfur, which precludes making conclusive statements based solely on its reactivity. Moreover, in the study by Cao et al.[7], tert-butanol (TBA), an atomic hydrogen scavenger, was added to the aqueous suspensions of nZVI and S-nZVI. Based on the observation that TBA greatly inhibited the reactivity of nZVI but not S-nZVI, they concluded that atomic hydrogen is generated on the iron (hydr)oxides site.

Thus, the atomic hydrogen theory production by S-nZVI is debatable. The objective of this section was to adopt the SKIE methodology to assess the role of atomic hydrogen in reactions of selected chlorinated solvent compounds with S-nZVI in aqueous solutions. The aim is twofold: first, to reproduce the SKIE experiments with Pd-nZVI and 1,1,1,2-TeCA in order to verify the reliability of their results and secondly, to conduct a similar experiment with S-nZVI and trichloroethene (TCE) and carbon tetrachloride (CT). These two chlorinated solvent compounds are target compounds whose degradation mechanisms were further investigated in Chapter 3. The significance of this experiment lies in the fact that if the SKIE ratio (k_H/k_D) is sufficiently high, it could serve as a compelling direct experimental proof of the atomic hydrogen theory, as

established with Pd-NZVI by Xie and Ciwertny[5]. Furthermore, it was hypothesized that if the SKIE ratio is high under high sulfur dosage, this would indicate the presence of atomic hydrogen on iron sulfides sites. Conversely, if the SKIE value is high under low sulfur dosage, this would imply the existence of atomic hydrogen on iron (hydr)oxides sites.

2.2 Methods and Materials

2.2.1 Chemicals

The chemicals $FeSO_4 \cdot 7H_2O$ (> 99%) and $NaBH_4$ (powder, > 98%) were procured from MP Biomedical and Acros Organics, respectively. D_2O, Na_2S, K_2PdCl_6, 1,1,1,2-tetrachloroethylene, trichloroethene and carbon tetrachloride were purchased from Sigma-Aldrich. H_2 gas with a purity level of 99.999% was procured from Praxair. HPLC grade methanol and 1-butanol (99% purity), was purchased from Fisher Scientific which met the required standards for the study. Additionally, all experiments were conducted using ultrapure water with a resistivity greater than 18 MΩ·cm,

2.2.2 Synthesis

Synthesis of nZVI

nZVI was synthesized as reported elsewhere[13]. A solution of 0.3 M $FeSO_4 \cdot 7H_2O$ was mixed continuously under anaerobic conditions, and then 1.3 M $NaBH_4$ was added slowly at a rate of 5 mL/min using a syringe pump. The mixture was stirred for 30 minutes, and the resulting

suspension of nZVI was washed with DI water and methanol for three times respectively, dried using nitrogen, and kept in an anaerobic chamber for storage.

Synthesis of Pd-nZVI

A procedure from Xie and Ciwertny's[5] work was carried out to prepare Pd-nZVI. Specifically, to make nZVI suspensions with a concentration of 2 g/L, deoxygenated DI water and as-prepared nZVI was used, and the suspensions were sonicated for 30 seconds. Pd doping of the nZVI surface was achieved by adding a specific volume (ranging from 100 to 700 μL) of a stock solution of 0.5 mM K_2PdCl_6 prepared in 0.01 N HCl to 5 mL of the nZVI suspension that was already dispersed. Two weight percentages of palladium-nanoscale zero-valent iron (Pd-nZVI) were synthesized, specifically 0.05 wt% and 0.35 wt%, and were designated as "0.05-Pd" and "0.35-Pd", respectively.

After the addition of Pd, the nZVI was mixed vigorously on vortex mixer for 5 minutes, during which time the initially orange-colored supernatant turned clear, indicating that Pd had been lost from the solution and taken up into the nZVI. Pd-nZVI particles were freshly made every time before batch experiment.

Synthesis of S-nZVI

S-nZVI was synthesized using the method reported in a prior study[13]. A 1.7 M solution of $NaBH_4$ and a solution of Na_2S (0.016M and 0.16M) were mixed together and then slowly added drop by drop, at a rate of 5 mL/min over a 45-minute period, into to an aqueous solution of 0.3 M

$FeSO_4 \cdot 7H_2O$ that was continuously mixed under anaerobic conditions. This was followed by 30 minutes of mixing. The resulting S-nZVI were washed three times with water and methanol before being dried for 12 hours in an anaerobic chamber. The dried particles were then stored in sealed vials in the chamber until they were ready to be used. The nominal (dosed) S/Fe molar ratios used were 0.01 or 0.1 and were designated as "0.01-S" and "0.1-S", respectively.

2.2.3 Reactivity Experiments

The degradation experiments of TCE were conducted in 70 mL vials with butyl rubber septa that were crimp-sealed. All the reactions were carried out in a solution made of 25 mM HEPES buffer and 25 mM NaCl (to adjust ionic strength), which was titrated to a pH of 8 by dropwise addition of 10 M NaOH solution. H_2O and D_2O were used as solvents in the SKIE experiment. The samples were prepared inside the anaerobic chamber, and all solutions were purged with nitrogen before handling. In the reaction vials containing Pd-nZVI, a total aqueous volume of 30 mL buffer solution (either made of H_2O or D_2O), 40 mg of nanoparticles and 100 µL of 1M 1,1,1,2-TeCA stock solution were added. In the reaction vials with S-nZVI particles, a total aqueous volume of 30 mL buffer solution (either made of H_2O or D_2O), 40 mg of nanoparticles and 50 µL of 1M TCE or CT stock solution was added. To disperse the nanoparticles, the samples were sonicated for 1 minute, and the vials were mixed at 350 rpm using an orbital shaker at a temperature of 22 ± 1.0 °C. Two 100 µL aliquots of the headspace were taken periodically for separate analysis of H_2 and CHCs and products. The calibration standards were prepared by adding known quantities of the gas standard to reactors set up in the same way as the reactivity systems, but without the nanoparticles.

2.2.4 Hydrogen Uptake Experiment

The degradation experiments were conducted in 70 mL vials with butyl rubber septa that were crimp-sealed. All the reaction were also carried out in a HEPES buffer solution as described above. The samples were prepared inside the anaerobic chamber with a mixed gas of 3% H_2 and 97% N_2. To the reaction vials, 25 mL buffer solution, 40 mg of nanoparticles and 100 µL TCE solution were added so that TCE was stoichiometrically in excess of the reductant, Fe(0). To disperse the nanoparticles, the samples were sonicated for 1 minute, and the vials were mixed at 350 rpm using an orbital shaker at a temperature of 22 ± 1.0 °C. Hundred µL aliquots of the headspace was taken periodically for analysis of H_2.

2.2.5 Analytical Methods

Analysis of CHCs

A gas chromatograph (Agilent 7820A) fitted with a flame ionization detector and a GS-Q column (30 m × 0.53 mm, Agilent) was used to analyze both the CHCs and their degradation products. The carrier gas, helium, was used with a flow rate of 5 mL/min. The temperature of the oven was programmed to start at 60 °C for 3 minutes, after which it was increased to 200 °C at a rate of 40 °C/min and held at that temperature for 7.5 minutes. The injector temperature was set to 250 °C with a split ratio of 5, while the detector temperature was kept at 250 °C. Additionally, the air flow rate was 300 mL/min, and the H_2 flow rate was 30 mL/min.

Analysis of H_2

H_2 was analyzed by a gas chromatography (GC) coupled with a thermal conductivity detector (TCD, Agilent 7820A) using a HP PLOT Molesieve column (30 m × 0.53 mm × 50 µm, Agilent). Ar was used as the carrier gas with a flow rate of 2 mL/min. The oven temperature was constant at 50 °C and the detector temperature was set at 120 °C.

2.3 Results and Discussion

2.3.1 SKIE experiment with S-nZVI of TCE and CT

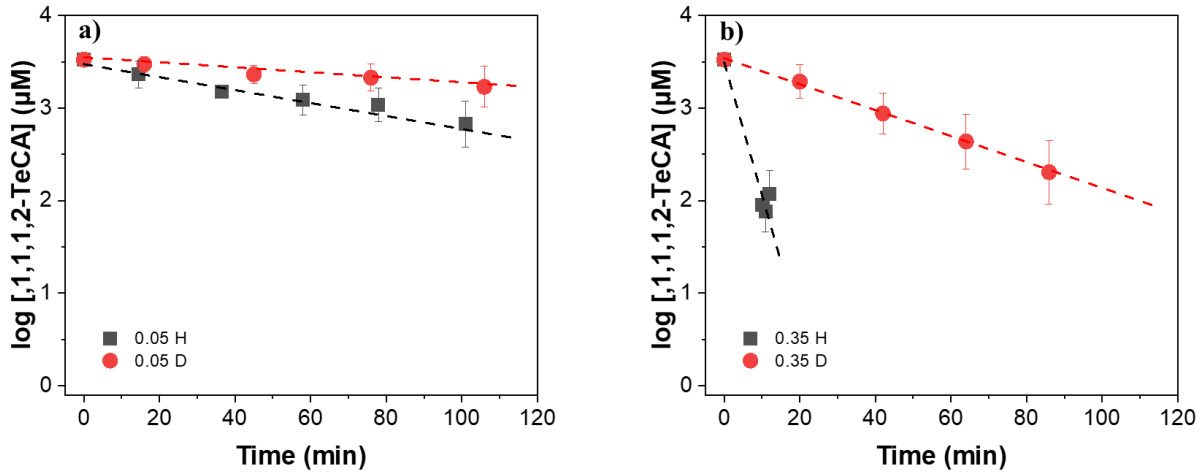

Figure 2-1. 1,1,1,2-TeCA degradation over time by (a) 0.05-Pd and (b) 0.35-Pd in the solvent of H_2O and D_2O.

Preliminary experiments successfully replicated the SKIE experiment of Pd-nZVI with TCE, previously reported by Xie and Ciwertny[5], as shown in Figure 2-1. Specifically, 0.05-Pd yielded a SKIE ratio of 2.59 (k_H = 0.007 min^{-1} and k_D = 0.0027 min^{-1}), while 0.35-Pd showed a SKIE

ratio of 10.25 (k_H = 0.1435 min^{-1} and k_D = 0.014 min^{-1}). The trends were similar to the Xie and Ciwertny[5] and verified the applicability of SKIE experiments to assess the involvement of atomic hydrogen during pollutant degradation.

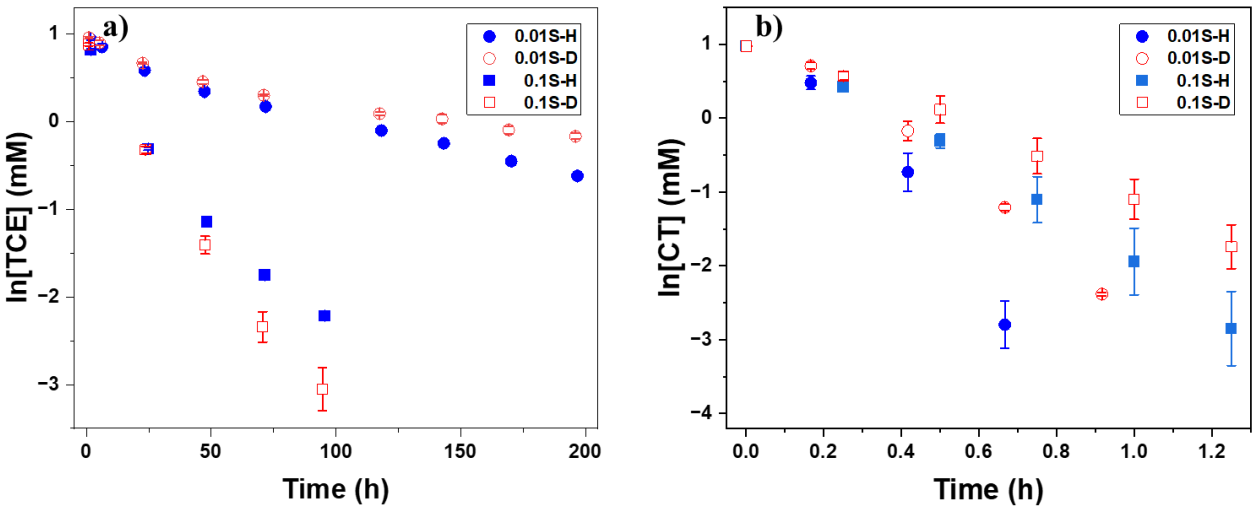

Figure 2-2. (a) TCE and (b) CT degradation over time by 0.01-S and 0.1-S in the solvents H_2O and D_2O.

Experiments were conducted with S-nZVI particles to further investigate the degradation mechanism of TCE and CT. TCE degradation by nZVI is believed to proceed via indirect atomic hydrogen transfer, while CT degradation is thought to occur via direct electron transfer, based on previous research by Li and Farrel[10]. Han and Yan[6] further proposed that the sulfur incorporated onto nZVI, serves as a site to efficiently produce atomic hydrogen that facilitates the TCE degradation on S-nZVI surface. The SKIE ratios obtained from Figure 2-2 for TCE, were 1.38 with 0.01S (k_H = 0.00723 h^{-1} and k_D = 0.00523 h^{-1}), and 0.76 with 0.1S (k_H = 0.03203 h^{-1} and k_D = 0.04213 h^{-1}). For CT, a SKIE ratio of 1.51 was obtained at 0.01S (k_H = 5.6453 h^{-1} and k_D = 3.7298 h^{-1}), and a SKIE value of 1.40 was obtained at 0.1S (k_H = 3.2709 h^{-1} and k_D = 2.3355 h^{-1}).

The above SKIE ratios suggest that atomic hydrogen presence and contribution to the degradation was not dominant. It should be noted that direct electron transfer and atomic hydrogen transfer pathways were observed with electrochemical experiments by Li and Farrel[10]. However, electrochemical experiments apply external electric fields, and the iron electrodes used in these experiments have different properties compared to iron nanoparticles used in this study. Therefore, the reaction mechanisms from the two types of experiments may differ.

Previous studies by Wei et al.[12] have also measured a small SKIE value for debromination by S-nZVI, which suggested that direct electron transfer rather than atomic hydrogen mediated reduction was the dominant pathway.

2.3.2 Hydrogen uptake experiment with Pd-nZVI and S-nZVI with TCE

Pd nanoparticles directly uptake hydrogen for dechlorination[8-9,11]. This phenomenon was also observed during Pd-nZVI batch experiments, where the total amount of hydrogen gas in the headspace decreased upon reacting with TCE. In order to investigate the hydrogen uptake ability of S-nZVI, a different set of experiments was conducted. Stoichiometrically excess TCE was introduced into vials to maximize hydrogen uptake, and a 5ml of butanol, that formed NAPL phase above the solution, was added to aid in particle adherence to the vial wall and increase exposure to the headspace gas. Figure 2-3 provides a visual representation of a typical vial from this experiment set.

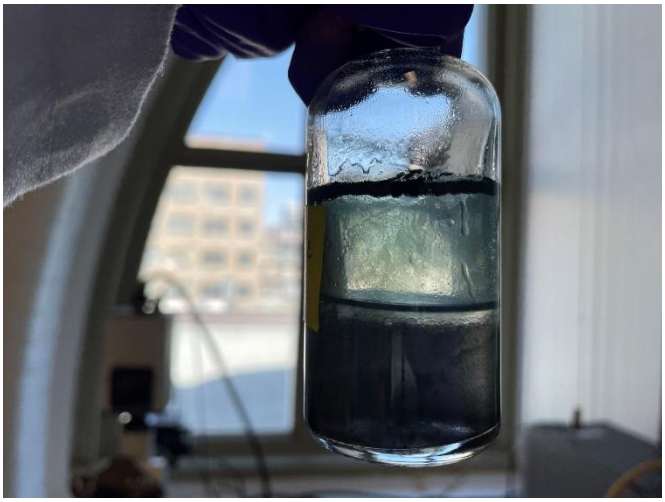

Figure 2-3. Particles were stuck on the vial wall and exposed to headspace for reaction.

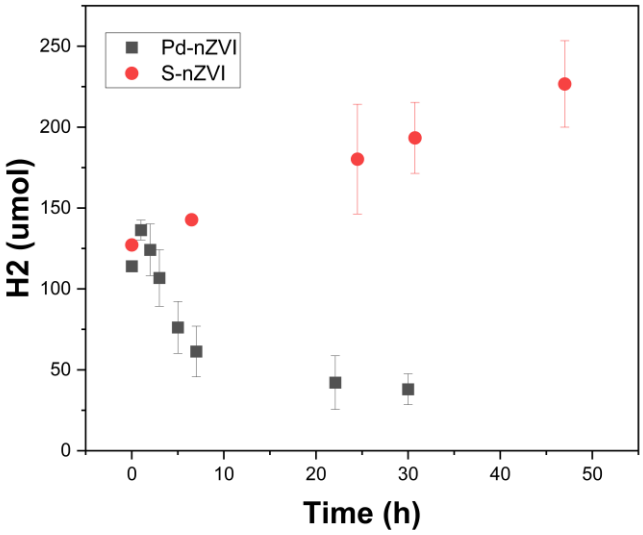

Figure 2-4. Hydrogen evolution time profile of 0.1-S and 0.35-Pd reacting with stoichiometrically excess TCE.

In Figure 2-4, it is evident that Pd-nZVI effectively uptakes hydrogen from the headspace. The hydrogen produced from iron corrosion reactions with water and from added H_2 is taken up and

converted to atomic hydrogen, which is then used in the hydrogenation reaction for TCE degradation, while S-nZVI does not exhibit the same behavior. In fact, there was net generation of H_2 by S-nZVI instead of hydrogen uptake over 120 hours of exposure.

Reference

[1] Carey, F. A., & Sundberg, R. J. (1984). Advanced Organic Chemistry: Part A: Structure And Mechanisms, 5Th Edition.

[2] Sykes, P. A (1986). Guidebook to Mechanism in Organic Chemistry; 6th ed.; Longman: Essex.

[3] Isaacs, N. S. (1987). Physical Organic Chemistry; Longman: New York.

[4] Melander, L., & Saunders, W. H. (1980). Reaction rates of isotopic molecules.

[5] Xie, Y., & Cwiertny, D. M. (2013b). Chlorinated Solvent Transformation by Palladized Zerovalent Iron: Mechanistic Insights from Reductant Loading Studies and Solvent Kinetic Isotope Effects. Environmental Science & Technology, 47(14), 7940–7948.

[6] Han, Y., & Yan, W. (2016b). Reductive Dechlorination of Trichloroethene by Zero-valent Iron Nanoparticles: Reactivity Enhancement through Sulfidation Treatment. Environmental Science & Technology, 50(23), 12992–13001.

[7] Cao, Z., Li, H., Lowry, G. V., Shi, X., Pan, X., Xu, X., Henkelman, G., & Xu, J. (2021b). Unveiling the Role of Sulfur in Rapid Defluorination of Florfenicol by Sulfidized Nanoscale Zero-Valent Iron in Water under Ambient Conditions. Environmental Science & Technology, 55(4), 2628–2638.

[8] Lowry, G. V., & Reinhard, M. (2001). Pd-Catalyzed TCE Dechlorination in Water: Effect of [H2](aq) and H2-Utilizing Competitive Solutes on the TCE Dechlorination Rate and Product Distribution. Environmental Science & Technology, 35(4), 696–702.

[9] Lowry, G. V., & Reinhard, M. (1999). Hydrodehalogenation of 1- to 3-Carbon halogenated organic compounds in water using a palladium catalyst and hydrogen gas. Environmental Science & Technology, 33(11), 1905–1910.

[10] Li, T., & Farrell, J. (2001b). Electrochemical Investigation of the Rate-Limiting Mechanisms for trichloroethylene and carbon tetrachloride reduction at iron surfaces. Environmental Science & Technology, 35(17), 3560–3565.

[11] Davie, M. G., Cheng, H., Hopkins, G. D., Lebrón, C., & Reinhard, M. (2008). Implementing heterogeneous catalytic dechlorination technology for remediating TCE-Contaminated groundwater. Environmental Science & Technology, 42(23), 8908–8915.

[12] Yin, H., Yin, H., Peng, H., Guo, Z., & Dang, Z. (2020). Sulfidation enhanced reduction of polybrominated diphenyl ether and Pb(II) combined pollutants by nanoscale zerovalent iron: Competitive reaction between pollutants and electronic transmission mechanism. Chemical Engineering Journal, 395, 125085.

[13] Bhattacharjee, S., & Ghoshal, S. (2018b). Optimal design of sulfidated nanoscale zerovalent iron for enhanced trichloroethene degradation. Environmental Science & Technology, 52(19), 11078–11086.

Chapter 3 Investigation of Active Sites in S-nZVI responsible for degradation of different chlorinated solvent compounds

3.1 Introduction

Zerovalent iron (ZVI) in its bulk, granular form has been used for groundwater remediation of halogenated organic pollutants since the 1990s[1-2]. With the development of nanotechnology in subsequent years, researchers have shifted their focus to its nano-scale form (nZVI) to obtain improved reactivity[3-6]. However, the high unintended reaction of nZVI with water has given rise to shortcomings of high nZVI dosage needs and poor selectivity to target pollutants. Among different surface modification methods to overcome these problems[7], sulfidation[8] is a very promising strategy by engineering an iron sulfides layer onto the Fe^0 core. S-nZVI has robust reactivity towards some chlorinated organic pollutants and limited reactivity to water. The minimized anaerobic corrosion with water is well illustrated by the surface hydrophobicity[9] or low affinity to water[30] of iron sulfides, but the mechanisms behind enhanced degradation of some contaminants (e.g., trichloroethene (TCE) and carbon tetrachloride (CT)) remains unclear.

Kim et al.[10] indicated that the iron sulfides shell acts as a bridge to transfer electrons from the iron core to the surface and these electrons are directly accessible to reduce adsorbed pollutant molecules (i.e., TCE). In contrast, Han and Yan[11] proposed that atomic hydrogen, an indirect electron transfer process, is formed on the iron sulfides because atomic hydrogen recombination to produce H_2 gas is poisoned at the surface and TCE is then reduced by the atomic hydrogen [12]. This hypothesis was not supported by Cao et al.[32] because they observed an apparent suppression in degradation rate of florfenicol with nZVI and no impact with S-nZVI in the presence of tert-

butanol (TBA), which is a scavenger for atomic hydrogen and hydroxyl radical[13-15]. One more recent hypothesis by Mangayayam et al.[25] suggests that the amount of reactive Fe^0 and FeS sites and inhibitory $Fe(OH)_2$ site present on S-nZVI surface control the degradation of TCE and cis-DCE with different sulfur doses, but no follow-up experimental proof were provided. Although these individual theories may explain experiment results with single pollutant or structurally very similar pollutants assessed in each of those studies, the extrapolation to others is impossible because these theories are somewhat contradictory to each other, which leads to a major knowledge gap.

One shortcoming in previous studies is that the particle characterization is always done before or after the reaction, but not during the reaction. Xu et al. measured the water contact angle and electron transfer resistance of S-nZVI particles to demonstrate the sulfur loading actually makes the particle more hydrophobic and provides a better conductivity. Additionally, morphology change of S-nZVI is always dramatic after the reaction[21]. Bhattacharjee[8] reported a big change in morphology of S-nZVI particles before and after reacting with TCE as a result of depletion of Fe^0 and outgrowth of iron oxide. How the particle morphology evolves during the reaction and the way sulfur affects this process is essential to understand S-nZVI reaction mechanisms comprehensively.

As discussed above, several studies[10-15, 25], proposed different mechanisms towards the enhanced reductive dechlorination of S-nZVI. However, all of them remain hypothetical due to the lack of direct evidence, and contradictory observations when applying on different CHC compounds. Another reason behind such a disagreement is the mismatch among experiment results from different groups. For example, in different studies the sulfur-induced degradation of carbon tetrachloride was reported to be either boosted, decreased or unaffected[11,17-18]. It is likely, that the

extent of impact on degradation by sulfidation depends closely on the S and Fe precursors, one-pot or two-pot procedure the actual sulfur dose and pollutant type[8-9,19-20]. Based on previous work from our group[8], the co-precipitated S-nZVI synthesized by Na_2S with best reactivity was selected, but different compounds have different optimal ratio of sulfur dose. Thus, the major objective is to develop a thorough theory to understand how sulfidation affects properties of nZVI and why degradation enhancement trend is different between CT and TCE with increasing sulfur dose. Preliminary solvent kinetic isotope effect (SKIE) experiments were carried out (Figure S1) and the result indicates no atomic hydrogen is involved, similar to observations by Yang et al[24]. A previous study[23] has demonstrated full inhibition of carbon tetrachloride degradation with zero valent iron by borate anion, forming bidentate-binuclear surface complex. Phosphate is another anion that exhibits similar behavior and is more prevalent in groundwater. However, it has been suggested that the presence of phosphate ions does not significantly hinder the efficiency of S-nZVI particles for TCE degradation[33]. This discrepancy is mysterious which is attributed to a lack of comprehensive research on the topic, necessitating a matrix of experiments to investigate the effect of phosphate on dechlorination by S-nZVI. The complexation of phosphate ions with the iron (hydr)oxides sites on the nZVI and S-nZVI surfaces can create inner sphere complexes, which renders the surface or part of the surface inactive for reaction and therefore demonstrate if the sites not bound by phosphates (i.e., Fe(0) or FeS) are active sites. Different species competition experiments were also carried out to verify an active site mechanism and a kinetic model was included to simulate the surface reaction of different CHC compounds on S-nZVI.

3.2 Methods and Materials

3.2.1 Chemicals

All chemicals used were the same as Chapter 2, except the disodium phosphate (Na_2HPO_4) was purchased from Fisher Scientific.

3.2.2 Synthesis

All the synthesis procedures of S-nZVI are the same as Chapter 2, which is one-step synthesis and 0.01-S, and 0.1-S were used.

3.2.3 Batch Experiments

The degradation experiments of TCE were conducted in 70 mL vials with butyl rubber septa that were crimp-sealed. All the reactions were carried out in a solution made of 25 mM HEPES buffer, 4.78 mM Na_2HPO_4, and 25 mM NaCl (to adjust ionic strength), which was titrated to a pH of 8 by 10 M NaOH solution. The samples were prepared inside the anaerobic chamber, and all solutions were purged with nitrogen before handling. A total aqueous volume of 30 mL buffer solution, 40 mg of S-nZVI and 50 μL of 1 M TCE or CT stock solution was added to the reaction vials. To disperse the nanoparticles, the samples were sonicated for 1 minute, and the vials were mixed at 350 rpm using an orbital shaker at a temperature of 22 ± 1.0 °C. Two 100 μL aliquots of the headspace were taken periodically for separate analysis of H_2 and CHCs and products. The

calibration standards were prepared by adding known quantities of the gas standard to reactors set up in the same way as the reactivity systems, but without the nanoparticles.

3.2.4 Analytical Method

The analysis of headspace gas composition follows the same procedure in Chapter 2.

3.2.5 Kinetic Model

Previous research suggests that competition among single species for limited number of surface reactive sites could occur during zerovalent iron (ZVI) reduction of organic pollutants and an adjusted Langmuir-Hinshelwood-Hougen-Watson (LHHW) model[34] was applied to model the kinetics of chlorinated ethylene and chlorinated acetylene with zerovalent iron, effectively[26]. In contrast to a typical catalytic reaction, the adapted model assumes irreversible reaction to simulate the dechlorination process and was demonstrated to be efficient in emulating the irreversible degradation of organic contaminants in TiO_2-facilitated photocatalysis[22,36]. Based on the reactive site theory proposed in this paper, a careful reasoning is provided later to justify the applicability of this model from ZVI to S-nZVI.

Assuming the mass transfer is rapid due to mixing, the LHHW model divides a surface reaction into three steps: 1) adsorption of substrate to surface reactive site, 2) surface reaction, and 3) desorption of product from surface and the dechlorination on S-nZVI can be controlled by any of the steps[34].

If the reaction is adsorption-limited and no inhibitor is present, the reaction rate is denoted by[26]

$$\frac{dC_i}{dt} = -\left(\sum_{j=1}^{N_j} k_{ij}^{a} S_t\right) C_i = -k_{obs} C_i \quad (1)$$

where C_i is concentration of chlorinated compounds (mM), k^a_{ij} ($mM^{-1} \cdot s^{-1}$)is the kinetic constant of the reaction whose rate determining step is adsorption, and S_t is the abundance of reactive site per unit volume of solution (mM). The subscript i represents the type of substrates and j represents the type of product. If the reaction converts CCl_4 primarily into $CHCl_3$, then the total number of product species (N_j) equals 1.

If the reaction is surface reaction-limited, the reaction rate is denoted by[26]

$$\frac{dC_i}{dt} = -\frac{\left(\sum_{j=1}^{N_j} k_{ij}^{s} S_t\right) K_i C_i}{1 + K_i C_i} = -k_{obs} C_i \quad (2)$$

where k^s_{ij} is the kinetic constant of the reaction whose rate determining step is surface reaction (t^{-1}), and K_i is the adsorption coefficient of parent compound (mM^{-1}).

If the reaction is desorption-limited, the reaction rate is denoted by[26]

$$\frac{dC_i}{dt} = -\left(\sum_{j=1}^{N_j} k_{ij}^{d} S_t\right) \quad (3)$$

where k^d_{ij} is the kinetic constant (s^{-1}) of the reaction whose rate determining step is desorption, and in this case, the reaction rate is no longer correlated to the initial substrate concentration. Since all batches showed a strong dependence of reaction rate and initial concentration, Equation 3 is not used hereafter.

3.3 Result and Discussion

3.3.1 Phosphate Ion Competition Experiments for S-nZVI with for Different Sulfur Doses and CHCs

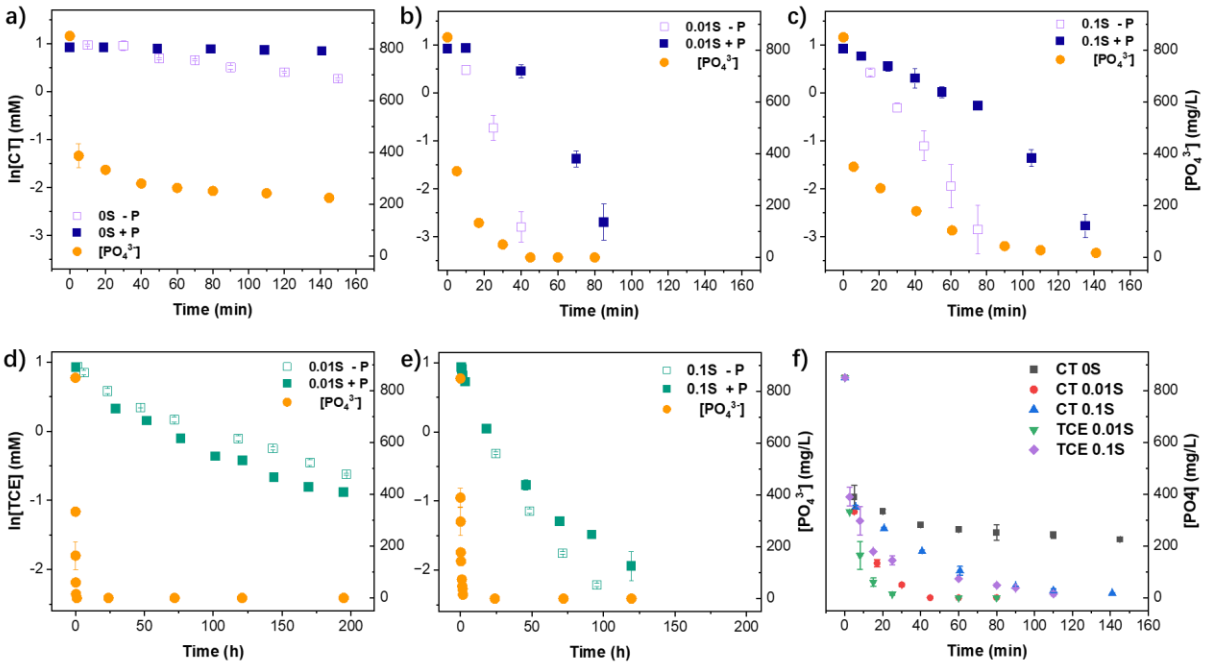

Figure 3-1. Phosphate ion competition experiment of (a) 0S with CT. (b) 0.01S with CT. (c) 0.1S with CT. (d) 0.01S with TCE. (e) 0.1S with TCE. (f) Aqueous phosphate level during first 160 minutes for all phosphate ion competition experiments

CHC degradation experiments were performed using nZVI (Fe/S molar ratios of 0) and two different doses of sulfidation of S-nZVI (Fe/S molar ratios of 0.01 and 0.1), denoted as 0S, 0.01S, and 0.1S, in order to evaluate its impact on the degradation of CT and TCE over time. The selection of these three doses was based on earlier findings in our group[35], indicating that the

optimal S/Fe ratio for CT degradation is 0.01, while that for TCE degradation is 0.1. Moreover, phosphorus can exist in three distinct states within the batch system. It may either be present in a dissolved state in the supernatant as [PO_4^{3-}], suspended in the supernatant as non-magnetic $Fe_3(PO_4)_2$, or adsorbed onto the surface of iron hydroxide particles as inner sphere complex, and a combined measurement by IC and ICP-OES was performed to determine phosphate species distribution in batches, as shown in Figure S10.

The degree of CT degradation suppression by phosphate was initially investigated using experiments with nZVI, as depicted in Figure 3-1 a. The observed rate constant (k_{obs}) for nZVI in the absence of phosphate was determined to be 3.2×10^{-1} h^{-1}, whereas in the presence of phosphate, it decreased significantly to 3.0×10^{-2} h^{-1}. This substantial reduction in the observed rate constant can be attributed to the rapid adsorption of the phosphate onto the nZVI surface and observed from the pronounced initial decrease in the phosphate level, as shown in Figure S10 a. However, the phosphate level did not exhibit further decline as the surface became saturated with coordination complexes of phosphate ligand, bringing them to a halt. Moreover, based on our previous research[20], we have established that chloroform (CF) serves as the primary reductive product of CT and its further dechlorination to dichloromethane (DCM) by S-nZVI is much slower. Therefore, the initial CF accumulation rate (Figure S2) can also demonstrate the extent of inhibition, which was 43.3 times slower. Herein, we have confirmed the surface phosphate complex on iron oxide layer of nZVI can suppress the CT degradation.

The presence of phosphate also exerted a substantial but different suppressive effect on CT degradation when using 0.01S and 0.1S (Figure 3-1 b, c). The kinetics for CT degradation exhibited a big change in slope of degradation curve for both 0.01S and 0.1S, primarily due to the coverage of the phosphate inner-sphere complex on the iron (hydr)oxides sites. For 0.01S, as

depicted in Figure 3-1 b, a noteworthy observation was that there was nearly negligible CT degradation during the initial 10 minutes in the presence of phosphate, attributed to the comprehensive coverage of the phosphate inner-sphere complex on the iron(hydr)oxide site. In contrast, a slow but consistent rate of CT degradation was observed during the initial 80 minutes for 0.1S, suggesting the impact of phosphate was less pronounced with 0.1S compared to 0.01S. This is expected, given that 0.1S would have more FeS sites than Fe(0) or $Fe(OH)_2$ sites. Furthermore, the decline in phosphate level was more rapid with 0.01S compared to 0.1S but both S-nZVIs eventually led to the complete depletion of aqueous phosphate species and subsequently facilitating the gradual recovery of the degradation rate constant, approaching to value under no-phosphate condition (Figure 3-1 bc).

Furthermore, we conducted another series of experiments to investigate the influence of phosphate on TCE degradation by S-nZVI, as shown in Figure 3-1 d, e. It should be noted that nZVI was excluded from these experiments due to its significant TCE adsorption capability. Despite the longer time scale required for TCE degradation compared to CT, the overall impact of phosphate ions on TCE degradation was found to be relatively minimal. Interestingly, for both 0.01S and 0.1S, the presence of phosphate even showed a slight enhancement in the early stage of TCE degradation, as shown in Figure 3-1 d and Figure S6. However, for 0.1S, after approximately 50 hours, the phosphate induced a tailing effect on the degradation curve between 70 h and 120 h, as evident in Figure 3-1 e. To gain further insights, we analyzed the hydrogen evolution profile presented in Figure S7. It was observed that the total amount of hydrogen generated in the presence of phosphate did not significantly differ from the scenario without phosphate. Considering that the amount of TCE being degraded also remained similar in both cases, it is unlikely that the tailing effect resulted from iron depletion due to reaction with water.

One possible cause of the observed tailing phenomenon is the formation of precipitated iron phosphate, which was confirmed in the TEM EDS image of 0.1S particles collected during the reaction, as shown in Figure S8. The formation of iron phosphate precipitates might lead to the encapsulation of some 0.1S particles, hindering the inward diffusion of TCE and the outward diffusion of Fe^{2+} ions. Consequently, this phenomenon could slow down both the TCE degradation and the hydrogen evolution in the later stages (i.e., after 50 hours), respectively.

3.3.2 An Active Site Mechanism Revealed by Phosphate Ion Competition Experiment

At pH 8, the majority of phosphate is present in the form of HPO_4^{2-} and would form inner sphere complex[28] that shields the iron (hydr)oxides active site, obstructing the association of CHC compounds to the surface and impeding the reaction.

For CT degradation, the limited amount of sulfur in 0.01S was not capable of forming substantial area of iron sulfides on the surface and one-step synthesis method allows sulfur to evenly distribute in the iron core. According to a pitting corrosion model developed by Marcus et al.[27], the presence of defects in lattice of Fe(0) lowers its corrosion resistance and therefore leads to an accelerated corrosion rate at the inter-granular boundaries of surface oxide layer. These FeS phases, acting as lattice defects, create particle structural instability during the pitting corrosion process in contact with water. Moreover, Gaspar et al.[37] reported visual evidence for such kind of pitting corrosion that happened between CCl_4 and granular iron (mZVI) that contravened previous assumption of uniform corrosion[38]. In this case, compared to granular iron, S-nZVI possesses iron sulfides phase that distributes over the whole particle structure, it would have

more nonuniform corrosion taken place when S-nZVI degrades pollutants. Therefore, the Fe^{2+} formed by corrosion either dissolves or precipitates, creates pitting or lattice dilatation, and de-passivate the particle surface. Afterwards, the newly exposed pure iron, as the second type of active sites, will directly adsorb aqueous phosphate ion, which can be proven by the sharp increase in phosphate adsorption by 0.01S at 30 min shown in Figure S10 b. For the case where there is no phosphate, Fe^0 site will react with CT and then form an oxide layer on the surface. This preferential reaction between newly exposed Fe^0 site and CT over water reduction can be supported by the observation that no hydrogen was produced when CT reacts with 0.01S (Figure S3). The oxide layer again served as extra iron (hydr)oxides site for more CT degradation to take place. The increase in number of active sites can also be verified by the CT degradation kinetics of 0.01S without phosphate that was assumed to be pseudo-first-order elsewhere[20]. While it is true that one reactant, Fe^0, is relatively excessive compared to the other, fulfilling the condition of pseudo-first-order, the first-order fit is not perfectly linear but is concave downwards, demonstrating more available active site.

Likewise, the enhanced CT degradation rate and faster phosphate consumption also happen to 0.1S, compared to 0S (Figure 3-1 c). Nevertheless, compared to 0.01S, the particle pitting corrosion process of 0.1S seemed mild (Figure 3-1 f), which might stem from the higher lattice stability of larger FeS phases high sulfur dose. It is noteworthy to mention the initial CT degradation with 0.1S and phosphate followed first order kinetics with a small rate constant, unlike 0.01S. This observation implies that iron sulfides are another active site for CT degradation because 0.1S contains enough sulfur to form abundant iron sulfides on the surface that cannot be hindered by phosphate. No discernible increase in first order rate constant during the first 80 minutes suggests limited amount of newly exposed iron sulfides site. Figure S10 c

also demonstrates particle pitting corrosion is relatively slow and mild because the drop in phosphate level is mainly through precipitation in the form of iron phosphate instead of adsorption, which is further confirmed by a TEM image (Figure S4).

Unlike nZVI (0S), the sulfidation could provide the particle with 1) iron sulfides sites, 2) iron (hydr)oxides site, and 3) exposed Fe^0, which get oxidized rapidly. As mentioned above, phosphate can only form inner sphere complex on either iron (hydr)oxides or Fe^0 site, therefore, no inhibition by phosphate to TCE degradation of 0.01S manifests that iron sulfides are the only active site. However, to explain the origin of degradation enhancement after adding phosphate, the idea of active site is insufficient. Unlike CT, TCE cannot outcompete water molecules, as illustrated in Figure S3 that the hydrogen evolution took place along with the entire TCE degradation process. Therefore, the side-reaction with water became important. We evaluated the by-reaction of water reduction that constantly competes for electrons with pollutants, as shown in Figure S5, and found adding phosphate suppressed the hydrogen evolution of 0.01S. It could be due to the passivation layer formed by phosphate inner sphere complex on surface, which benefits the preservation of electrons in Fe^0 core to be transported to iron sulfides site and thus boosts the TCE degradation indirectly. We also conducted the hydrogen evolution test (Figure S7) for 0.1S, which indicated there was an increase in hydrogen evolution compared to the case without phosphate. The observed variation between 0.01S and 0.1S was primarily caused by their different main sites reacting with water. Because of different sulfur doses, 0.01S transferred electrons mainly through iron (hydr)oxides site while 0.1S did it mainly through iron sulfides site. The introduction of phosphate complex can easily decelerate the water reduction for 0.01S, but not for 0.1S. Conversely, the phosphate could accelerate the pitting corrosion process of 0.1S by precipitation. Since the system was buffered at basic pH value, the particle surface is mainly

surrounded by OH groups without phosphate. After nZVI released electrons, Fe^{2+} or Fe^{3+} ion was released after reaction with water, a relatively soluble $Fe(OH)_2$ (K_{sp} = 7.9E-15) was formed compared to $Fe_3(PO_4)_2$ (K_{sp} = 1.0E-36) in the presence of phosphate because phosphate concentration was much higher than hydroxide concentration. The precipitation of Fe^{3+} species is not considered because iron corrosion potential in anoxic water is negative compared to standard hydrogen electrode and pH is above 7, so based on the Pourbaix diagram of Fe, most precipitated iron species on particle surface have a valence state of 2. As a result, the reacted iron was more ready to either leave the core or form iron phosphate, and the accelerated pitting corrosion facilitated exposure of inner iron sulfides active sites, leading to a faster degradation rate of TCE in the early stage. In general, the pseudo-first-order kinetics of TCE degradation is slightly concave upwards without phosphate (Figure 3-1 d, e), which is evidence of deactivation of particles as more and more iron in the core was depleted in the long term. An additional explanation lies in the potential of iron phosphate to accelerate the degradation of TCE through dual impact of adsorption and reduction. As reported by Li et al.[16], their result revealed that the phosphorization of microscale zero-valent iron enhanced its chemical reductive capacity for TCE. Moreover, it was observed in that study that iron phosphate, when present in aqueous solutions, possess the ability to adsorb TCE molecules.

Consequently, multiple factors, encompassing the formation of suspended iron phosphate species, the substitution of iron (hydr)oxides surface sites with iron phosphate, and the accelerated pitting corrosion that led to faster hydrogen evolution rate and more iron sulfides site, collectively resulted in the changes of TCE degradation kinetics by S-nZVI in the presence of phosphate. Importantly, none of these scenarios manifested an inhibitory effect akin to the one observed in CT degradation experiments induced by phosphate ions.

Different active sites are responsible for degrading different pollutants, while the enhanced CHC degradation suggests pitting corrosion leads to localized breakdown of S-nZVI particles that creates more active sites during the reaction. The iron sulfides are the only active site for TCE degradation, while iron sulfides site, iron (hydr)oxides site, and exposed Fe^0 site are active sites for CT degradation. Because of the instantaneous transformation of Fe^0 site into iron (hydr)oxides site, Fe^0 site's contribution to degradation is counted as part of iron (hydr)oxides site hereafter. In other words, TCE degradation occurs on iron sulfides site while CT degradation occurs on both iron sulfides site and iron (hydr)oxides site. Since TCE and CT can both be degraded on iron sulfides site, a series of inter-species competition experiment between TCE and CT on S-nZVI was further conducted to testify this theory.

3.3.3 Inter-species Competition Experiment of S-nZVI between CT and TCE

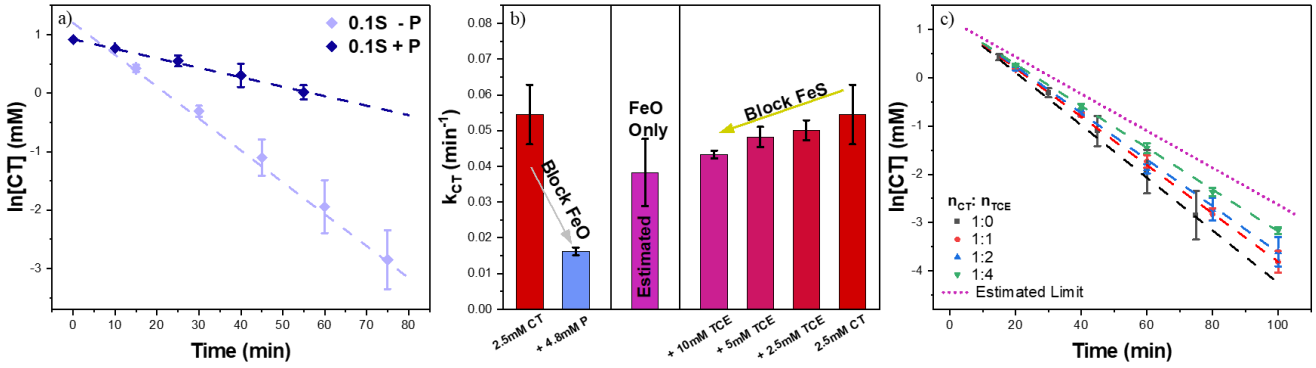

Figure 3-2. (a) Initial stage of CT degradation with and without the presence of phosphate by 0.1S (fitted by pseudo-first-order kinetics). (b) Comparison of pseudo-first-order rate constants

for the degradation of CT by 0.1S with coexistence of phosphate or different amount of TCE. (c) Inter-specie competition experiment of 0.1S between CT and TCE.

The active site theory manifested from phosphate competition data for S-nZVI reveals the origin of different batch reactivity for different sulfur dose, which also implies the possible competition for iron sulfides site between CT and TCE. Based on the general kinetic observation in last section, CT was selected as the target compound for its rapid degradation compared to TCE, which was selected as the potential competitor. In addition, 0.1S had relatively faster TCE degradation rate and slower CT degradation rate compared to 0.01S. Thus, we expected observable TCE disappearance would occur before all the CT was degraded and 0.1S was therefore selected for further inter-species competition experiment to testify the proposed active site theory.

For 0.1S, pitting corrosion is minor, so iron sulfides are the major active site in the presence of aqueous phosphate while the iron (hydr)oxides site is obstructed. Hence, in Figure 3-2 a, the rate disparity was a result of exclusive CT degradation on iron (hydr)oxides site and by subtracting from each other, an estimated degradation rate constant of iron (hydr)oxides site on 0.1S can be achieved (Figure 3-2 b). Since main TCE degradation is hypothesized to happen on iron sulfides surface, in principle, it would compete with CT for electrons on iron sulfides site despite its slower degradation kinetics than CT. In Figure 3-2 c, the result demonstrates that the coexistence of TCE did retard the CT degradation and by raising the TCE concentration to four times higher than CT, the rate constant (i.e., 4.3×10^{-2} min^{-1}) was only 13% higher than the estimated limit (i.e., 3.8×10^{-2} min^{-1}).

As shown in phosphate competition section (Figure S7), the blockage of iron (hydr)oxides site did not enhance the TCE degradation by 0.1S significantly, which demonstrated there is no non-reactive competitive adsorption of TCE on iron (hydr)oxides site and TCE was only selectively absorbed on iron sulfides site. Thus, the addition of TCE did not influence the accessibility of CT on iron (hydr)oxides site and the decrease in the rate constant was mainly due to the competition of iron sulfides site between two chlorinated compounds. Since more TCE is replacing CT on the iron sulfides site and it possesses larger molecule size and slow degradation kinetics than CT, it is reasonable to expect a decrease in total electron utilization rate.

The total reaction time was controlled within 100 minutes, so the electrons taken by further conversion of primary products (i.e., chloroform and acetylene) into secondary products (i.e., dichloromethane and ethene) were negligible. The electron stoichiometry in our laboratory's previous work[20] indicates 1 TCE molecule requires 2 electrons to be converted into acetylene while 1 CT molecule only requires 1 electron to be converted into chloroform. Hence, by multiplying the initial concentration with first-order rate constant and electron number respectively, and add them together, the initial electron utilization rate can be computed, as shown in Figure S9. However, the data demonstrated that the coexistence of TCE in batches did not influence the electron utilization rate and the required retention time per unit of electron of TCE on iron sulfides site is not significantly longer than CT, given that the number of CT and TCE molecules per unit of area are similar (molar volume of CT = 96.7 cm^3/mol, and TCE = 90.2 cm^3/mol). One assumption needs to make here is single adsorption layer of CHC molecule on particle surface for reduction to take place. In turn, the CT degradation kinetics is slowed on iron sulfides site compared to other sites, which can also be confirmed by the large inhibition by phosphate considering the majority of 0.1S surface consists of iron sulfides (Figure 3-1 c). The

blockage of phosphate can only affect very small portion of 0.1S surface, but the inhibition is obvious. Nevertheless, this cannot explain the enhanced CT degradation by 0.1S than normal 0S because the more iron sulfides on the surface should lead to a drop in the degradation rate. One possible explanation is that the incorporated sulfur mitigates the passivation. Gu et al.[29] reported the mechanism of mitigated passivation by incorporating sulfur onto micro-size zero valent iron (S-mZVI). The SEM image showed reacted S-mZVI particle had a puffy surface that pristine mZVI did not have and such a structure facilitated the contact between pollutant and particle even at pH 9-10 where mZVI lost dechlorination ability. Unfortunately, neither SEM nor TEM technique can help with nano-size particles to obtain visual evidence for verifying pitting corrosion and mitigated passivation because the outgrowth of oxide layer after reaction make the particle look blurry (Figure S11, 12). Anyway, the enhanced CT degradation of S-nZVI than nZVI proves, to great extent, an increase in number of exposed active sites caused by pitting corrosion. In addition, all the experiments in this study were conducted in a buffer of pH 8 and the particle reactivity was not noticeably lower than the previous unbuffered system in our group, which also proves the passivation on 0.1S is mitigated by sulfur.

To sum up, the most important information can be added to the proposed mechanism is that CT degradation is extremely slowed on iron sulfides site than that on iron (hydr)oxides site. Likewise, another hypothesis that a change in rate determining step of CT degradation can be made. Therefore, intra-species competition experiment coupled with Langmuir-Hinshelwood-Hougen-Watson (LHHW) model were used to find out the rate determining step of CHC reduction on two different sites.

3.3.4 Intra-species Competition Experiment of S-nZVI between CT and TCE

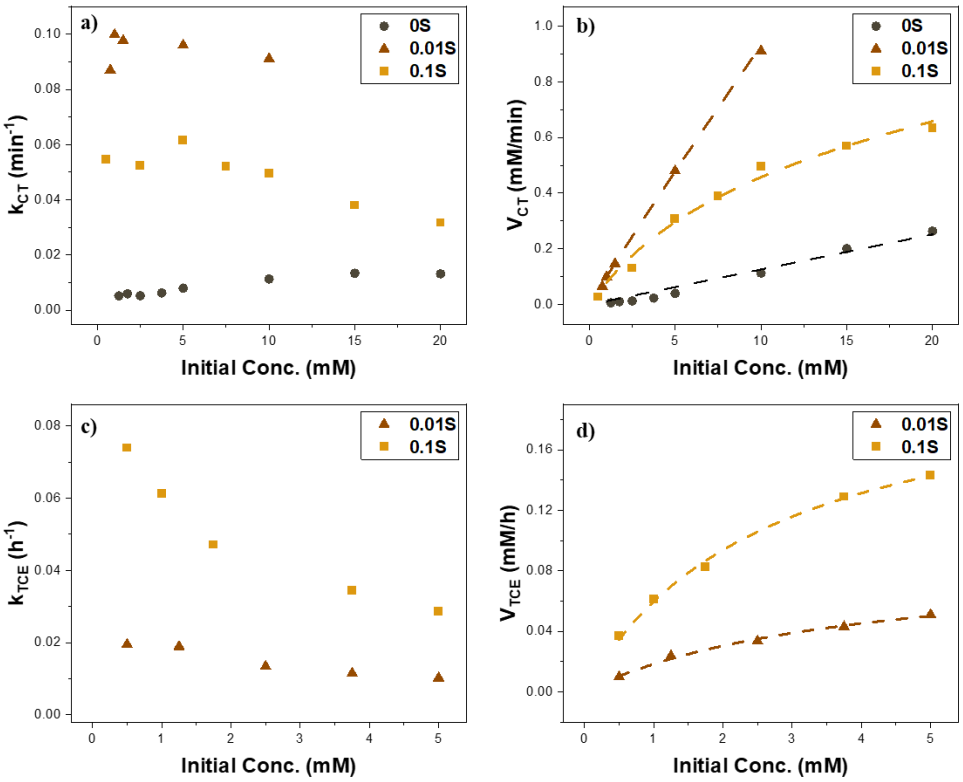

Figure 3-3. The reaction rate constant and initial reaction rate of 0S, 0.01S, 0.1S with CT (a,b) and with TCE (c,d). The dashed lines are regression results from LHHW model,

A systematic investigation was conducted to study the relationship between initial concentrations and pseudo-first order reaction constant and all the intra-species experiments were conducted within a limited time period (i.e., TCE – less than 40 hours; CT – less than 2 hours) so that the major degradation product of TCE is acetylene and that of CT is chloroform to meet the LHHW model requirement. Most results in Figure 3-3 ac demonstrated a strong dependence between concentration and rate constant. For instance, the reaction rate constant decreased by a factor of 3 with a slight increase in initial concentration to 5mM. One thing to note is that this is the first

report on the intra-species competition of S-nZVI degrading TCE and most studies considered the BET surface area as the only variable of rate constant[8, 30-31]. Nevertheless, such a dependence of 0S (Figure 3-3 a) was opposite that the rate constant was positively correlated to the initial CT concentration. Similar phenomenon was also observed by Johnson et al.[23] and it was mainly due to the enhanced corrosion under a higher chloride level as the basic environment could easily passivate the iron surface.

By multiplying the rate constant value with corresponding initial concentration, the value of initial reaction rate can be achieved, as shown in Figure 3-3 bd. Despite the slight increase in rate constant of 0S with a higher initial CT concentration, the overall trend of initial reaction rate was linear. In contrast, the initial reaction rate of S-nZVI, especially 0.1S, showed a polynomial nonlinear curve of for CT degradation (Figure 3-3 b). Recalling that in last section, a conclusion that iron sulfides surface, compared to iron (hydr)oxides surface, significantly decelerated CT degradation was drawn. Thus, such a change in shape was caused by a transformation from adsorption-limited type to surface reaction-limited case with higher sulfur dose. In other words, the kinetics of CT degraded on iron sulfides site is surface reaction-limited type while that on iron (hydr)oxides site is adsorption-limited type. The adapted LHHW model was applied to fit the datapoint in Figure 3-3 b and formula 1 was used to fit 0S while a combination of formula 1 and 2 was used to fit 0.01S and 0.1S. For TCE (Figure 3-3 d), no linear relationship was observed at both high and low sulfur doses, formula 2 was used to fit 0.01S and 0.1S to model the surface reaction-limited TCE degradation on iron sulfides site exclusively. All the computed parameters are provided in Table 3-1.

Table 3-1. Computed LHHW model parameters for TCE and CT degradation by 0S, 0.01S and 0.1S

CT	$(k_{ij}^{a}S_t)$ (min^{-1})	$(k_{ij}^{s}S_t * K_i)$ (min^{-1})	K_i(mM^{-1})
0S	0.01261 (6.216E-4)	N/A	N/A
0.01S	0.08651 (0.01139)	0.01512 (0.01293)	0.13129 (0.05407)
0.1S	0.00897 (0.01786)	0.07934 (0.00793)	0.11580 (0.07934)
TCE	$(k_{ij}^{a}S_t)$ (h^{-1})	$(k_{ij}^{s}S_t * K_i)$ (h^{-1})	K_i(mM^{-1})
0.01S	N/A	0.0231 (0.00213)	0.26133 (0.00213)
0.1	N/A	0.08174 (0.00481)	0.37241 (0.03889)

*Values in brackets represent 95% confidence limits

The adsorption-limited degradation of CT on iron (hydr)oxides sites was presented by the lumped constant [k^aS_t]. The 1% sulfur dose resulted in 7 times faster degradation than pristine nZVI, primarily due to the larger surface area resulting from the rapid oxidation of Fe^0 sites to iron (hydr)oxides after pitting corrosion. At high sulfur dose, the majority of particle surface is made of iron sulfides but the drop in contribution by iron (hydr)oxides site is not that much, which again indicates there is pitting corrosion happening on 0.1S, but mild. For the surface reaction-limited CT degradation on iron sulfides site, the two adsorption parameters K_i were similar to each other, indicating the degradation type is the same, which makes the comparison of

lumped constant [k^sS_t] valid. According to the fitted result in Table 3-1, the [k^sS_t] value of 0.1S is 5.24 times larger than 0.01S, suggesting that the area of iron sulfides active site on 0.1S is around 5.24 times more than that on 0.01S. It is worth mentioning that, if the real adsorption constant is too small (i.e., <<1), the CT degradation on iron (hydr)oxides site could also be surface reaction-limited, which is the same as that on iron sulfides site. Nevertheless, no matter whether there is a change in rate determining step of CT degradation on different sites or not, the fitting result clearly demonstrated a shift in reaction kinetics with higher sulfur dose.

In contrast, the computed adsorption constants for TCE degradation are not the same for 0.01S and 0.1S. According to the active site theory developed so far, the TCE degradation should only occur on iron sulfides site, indicating similar adsorption constants is expected to compute. Such a variation in adsorption constants was mainly ascribed to the ignored contribution of iron (hydr)oxides site on TCE degradation. The result in Figure 3-1 e showed a combined effect of adding phosphate within first 20 hours, including both negative effect (i.e., obstruction of phosphate on iron (hydr)oxides site) and positive effect (i.e., accelerated pitting corrosion by phosphate (Figure S7)), which made us draw a wrong conclusion at first place that TCE degradation happened on iron sulfides site exclusively.

Considering the majority of 0.1S surface is iron sulfides site and slow TCE degradation on iron (hydr)oxides site, the adsorption constant [K_i] can be seen as an approximation of the actual adsorption constant of TCE on the iron sulfides sites. Thus, an estimation of the kinetic parameters of TCE degradation on iron (hydr)oxides site of 0.01S can be achieved. To be specific, the lumped constant [$k^sS_t*K_i$] and adsorption constant [K_i] of 0.01S can be divided into two parts, iron sulfides site and iron (hydr)oxides site. The adsorption constant of TCE on iron sulfides site can be referred to the value obtained from 0.1S, the abundance of iron sulfides site

[S_t] is 5.24 times less than 0.1S, and solving the equation gives results shown in Table 3-2. It is evident that despite the much higher abundance of iron (hydr)oxides site than iron sulfide site, the reaction kinetic constant [k_s] is much slower than the TCE degradation on iron sulfide site. At the meantime, the adsorption constant of TCE on iron (hydr)oxides site is also smaller than that on iron sulfides site, suggesting a slower adsorption process. Hence, these two factors explain the superior degradation performance of TCE brought by S-nZVI. W. Arnold[26] also reported a surface-limited type of TCE reduction on mZVI that coincides, but we could not reproduce with 0S because their particle size was 150 microns and ours was less than 1 micron, which possibly led to massive TCE adsorption.

Table 3-2. Computed LHHW model parameters for TCE degradation by FeS on 0.1S and estimated value by two different sites on 0.01S

TCE	$(k_{ij}^{s} S_t * K_i)$ (h^{-1})	K_i (mM^{-1})
FeS_0.1S	0.08174	0.37241
FeS_0.01S	0.01560	0.37241
FeO_0.01S	0.0079	0.1434

One thing to note is that, since the reaction rate depends closely on the CHC concentration as well as the kinetic parameters of different site with a certain type of CHC compound, the reaction rate constant does as well. So, this gives a possible factor that leads to the mismatch on experiment results among different groups.

Supplementary Information

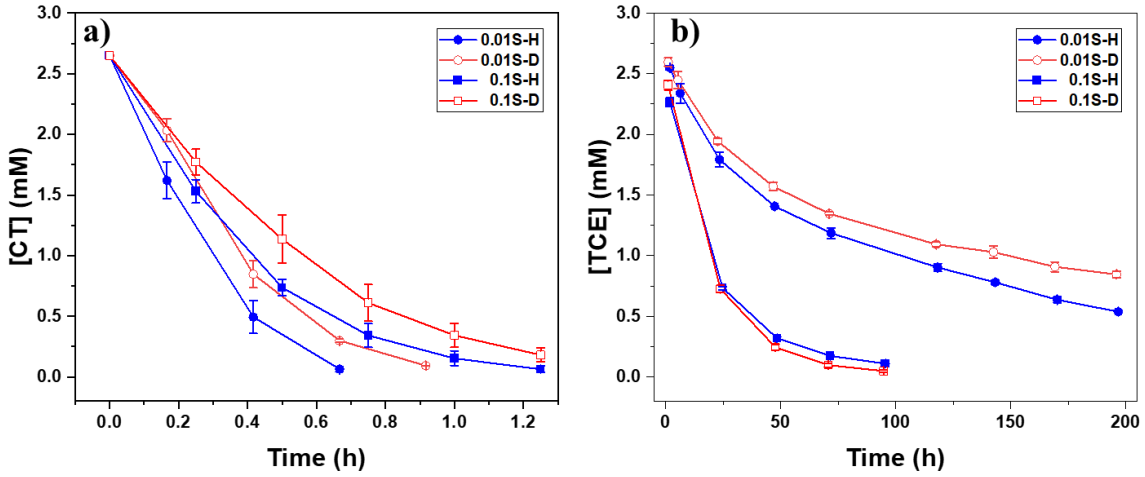

Figure S1. Degradation curve of a) CT, and b) TCE by S-nZVIs with low and high sulfur dose in the solvent of H_2O and D_2O. The involvement of atomic hydrogen during degradation would lead to a prominent deviation in degradation rate, which is explained by solvent kinetic isotope effect.

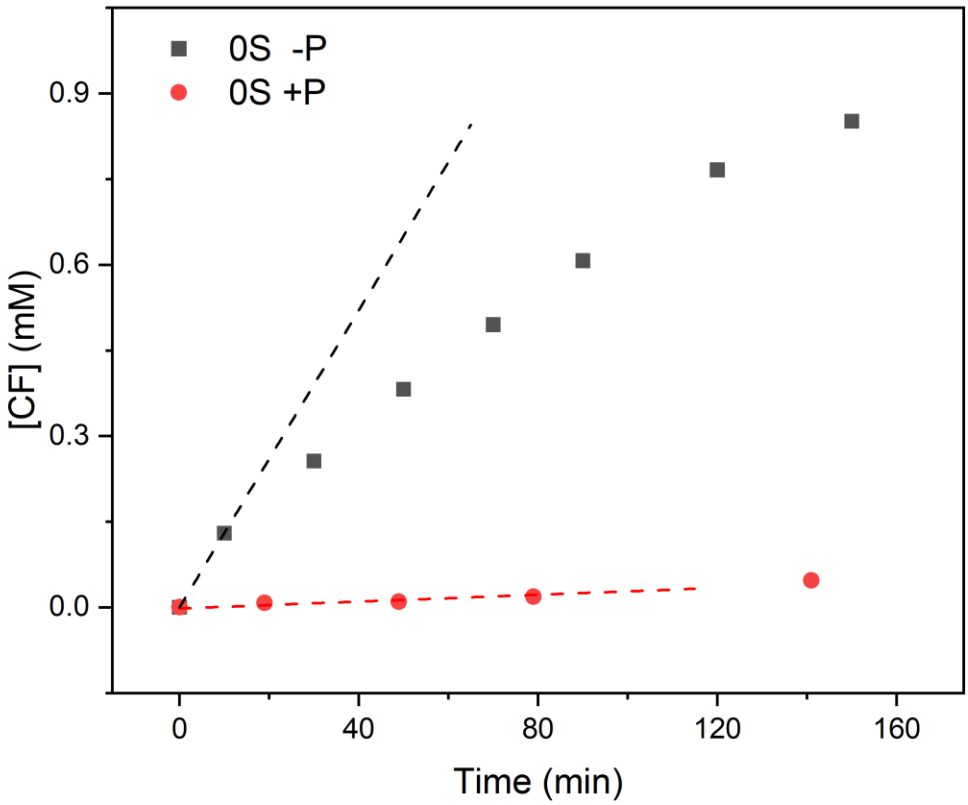

Figure S2. Chloroform accumulation profile for nZVI reacting with CT with and without phosphate

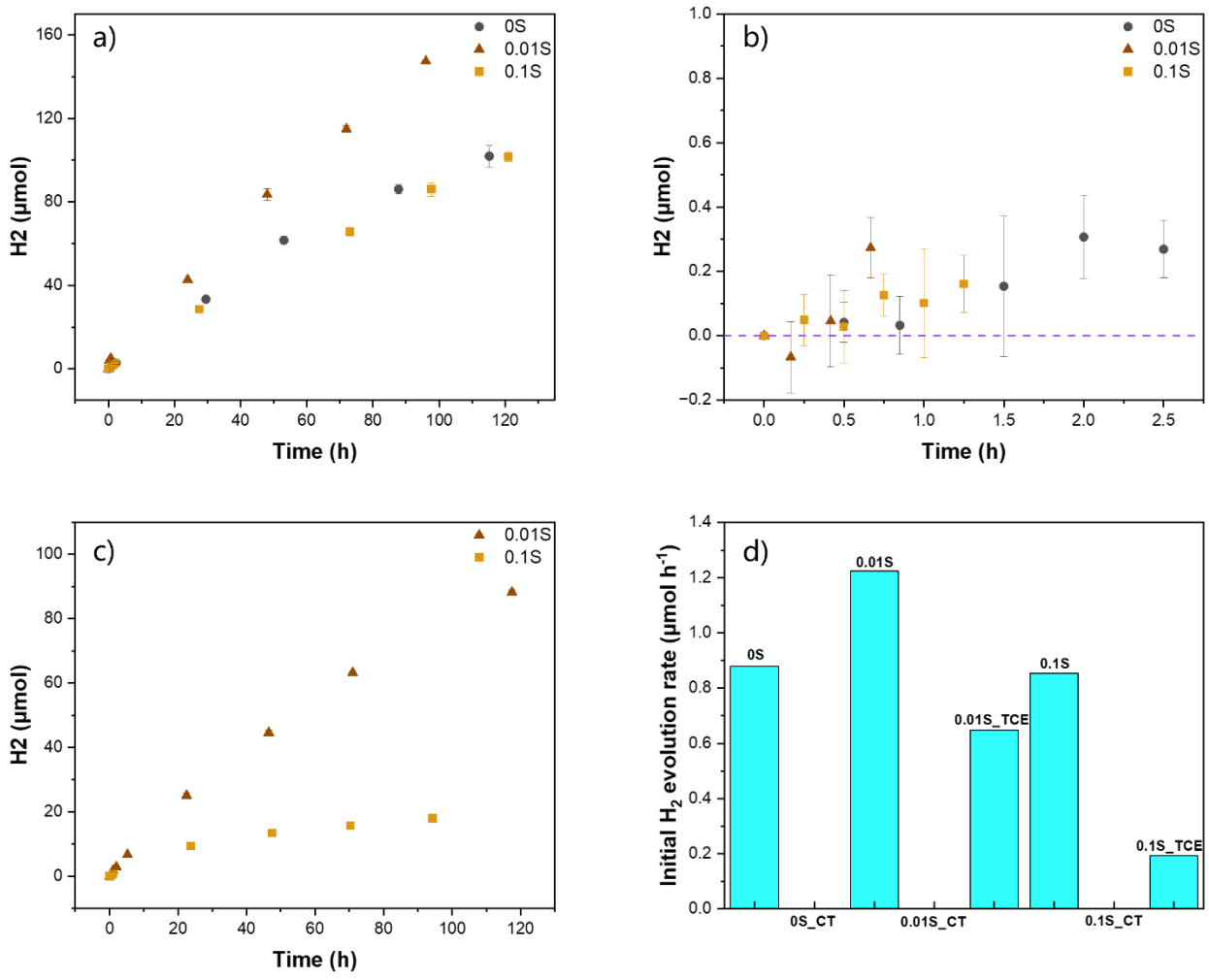

Figure S3. Hydrogen evolution profile of S-nZVI with different sulfur dose in absent of phosphate where a) no pollutant; b) 2.5mM of carbon tetrachloride with a purple dashed line serving as zero point; c) 2.5mM of trichloroethene is present. And d) is a summary of the initial hydrogen evolution rate for each scenario.

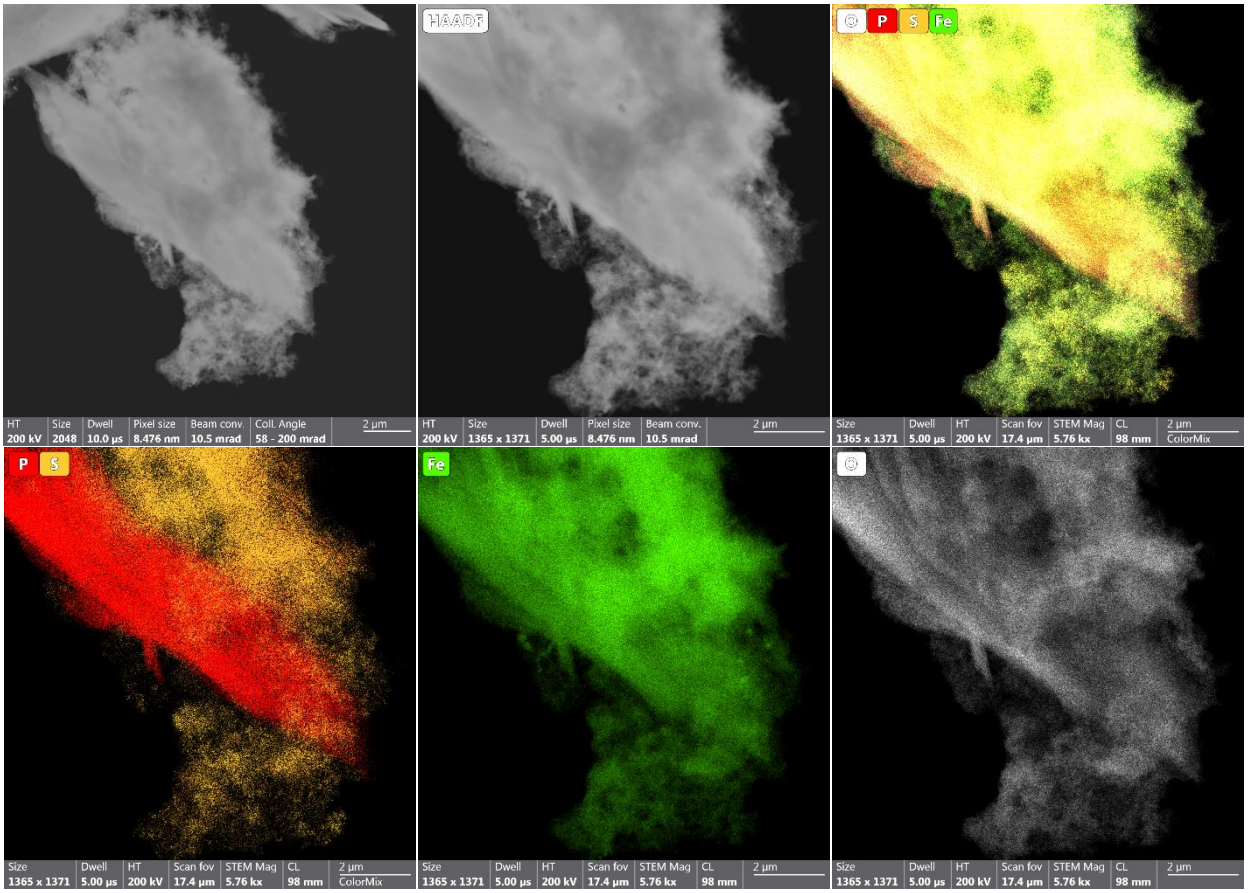

Figure S4. HAADF image and element mapping of a iron phosphate piece intertwining with amorphous iron sulfide collected from supernatant after 0.1S reacted with 2.5mM CT in the presence of phosphate for 20 min.

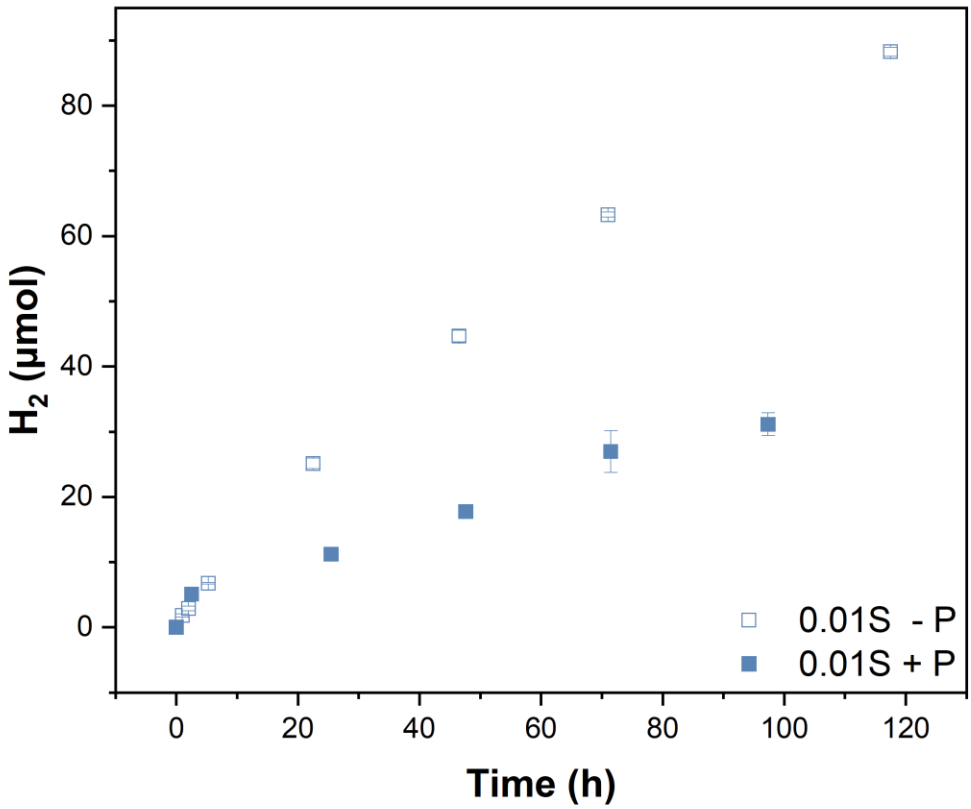

Figure S5. Hydrogen evolution profile of 0.01S reacting with 2.5 mM TCE with and without phosphate.

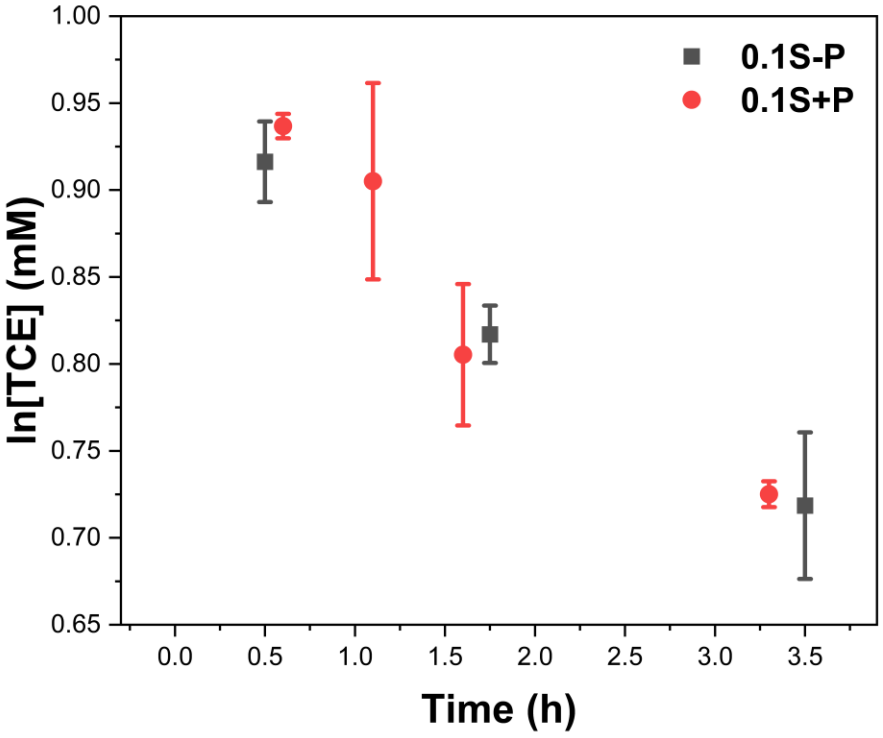

Figure S6. TCE degradation profile by 0.1S with and without phosphate during the early stage

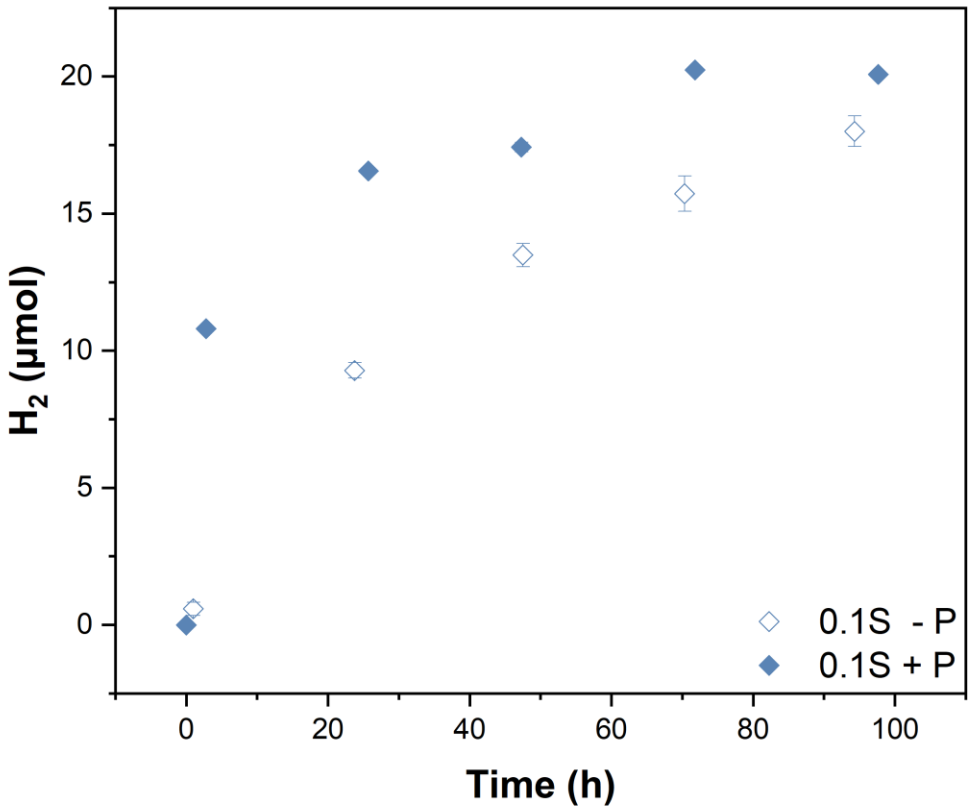

Figure S7. Hydrogen evolution profile of 0.1S reacting with 2.5 mM TCE with and without phosphate.

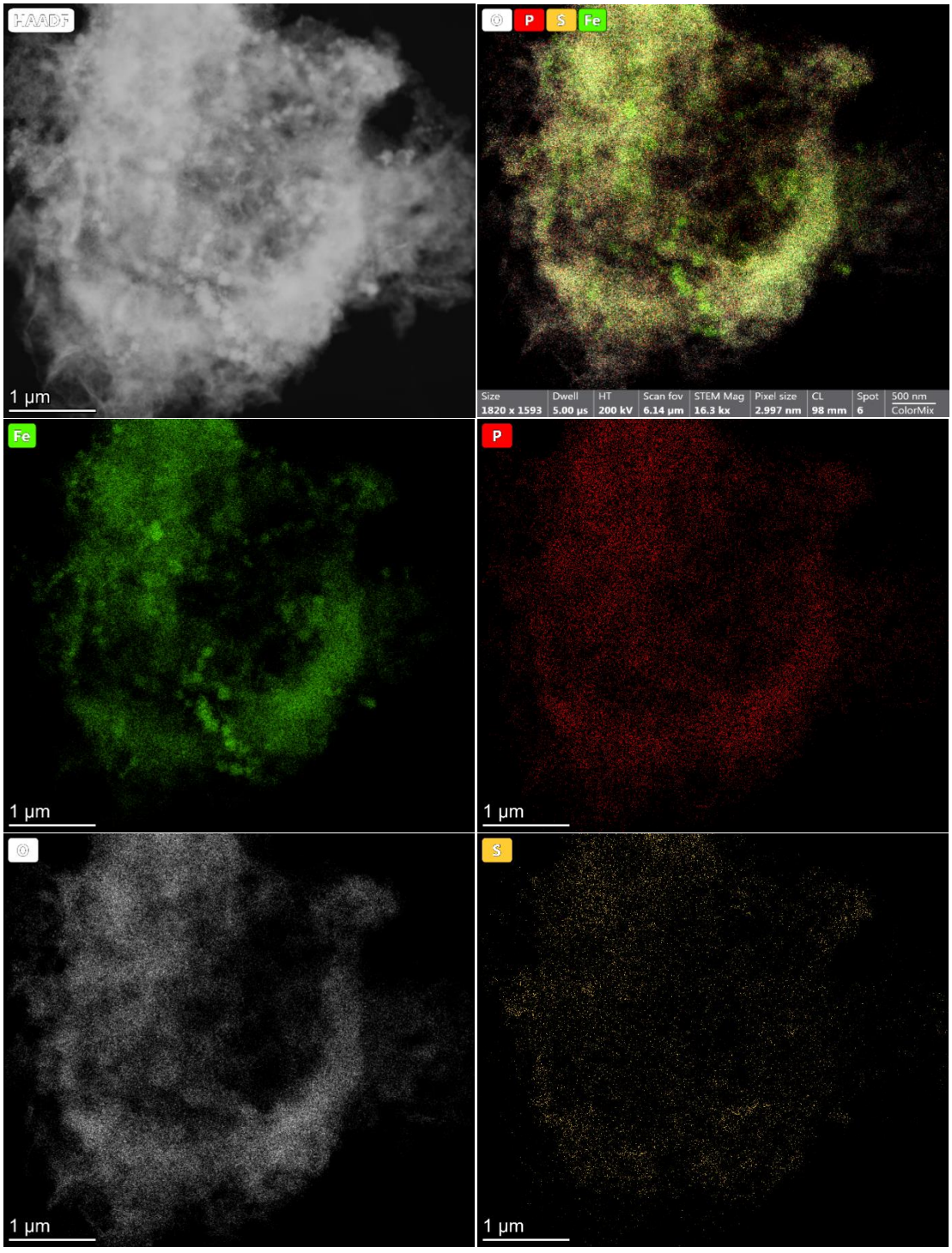

Figure S8. HAADF image and element mapping of a iron phosphate chunk wrapping some nanoscale 0.1S particles collected from supernatant after 0.1S reacted with 2.5mM CT in the presence of phosphate for 100 min.

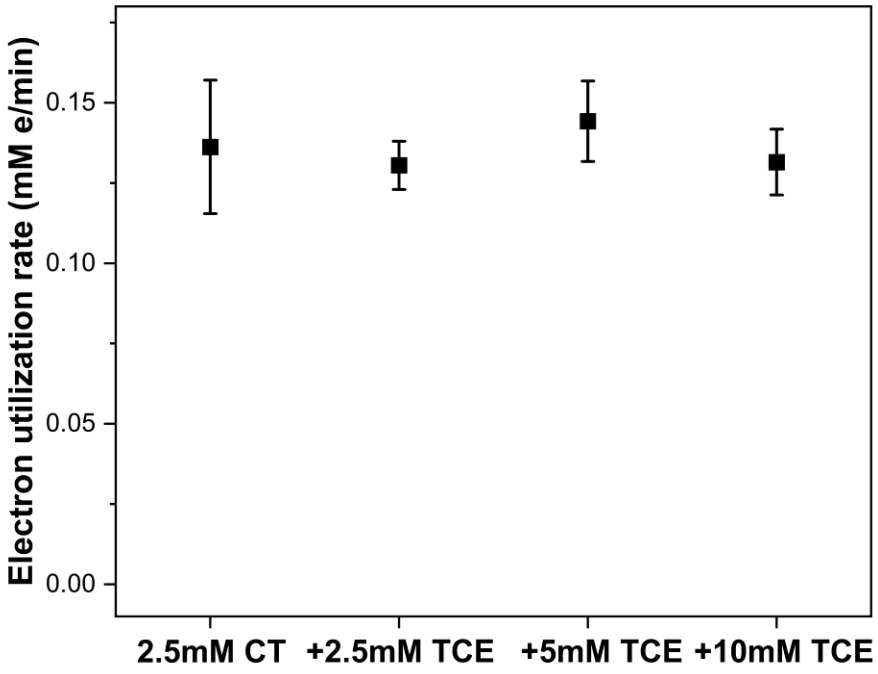

Figure S9. Computed initial electron utilization rate of all four inter-specie competition experiment.

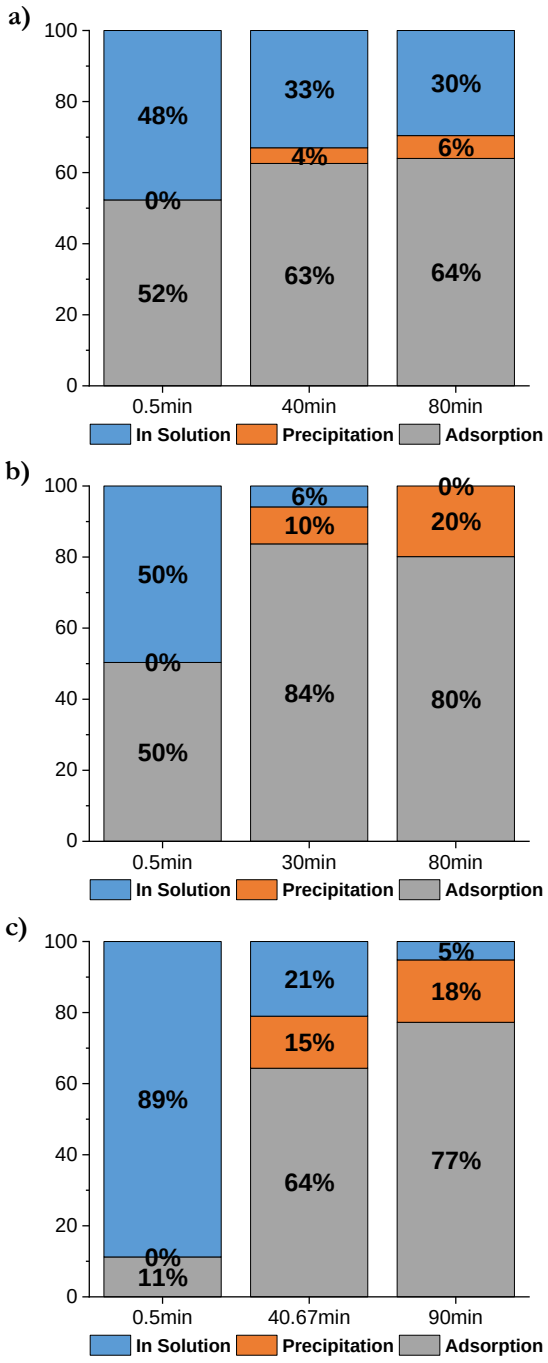

Figure S10. Phosphate species distribution in batch experiments for a) 0S reacting with CT, b) 0.01S reacting with CT, and c) 0.1S reacting with CT. The IC measurements determined phosphate aqueous concentration in the solution while ICP-OES measurements determined both

aqueous and solid (i.e., $Fe_3(PO_4)_2$) state of phosphate. It was assumed that no precipitation took place at 0.5min and ICP-OES measurements represented aqueous concentration of phosphate exclusively.

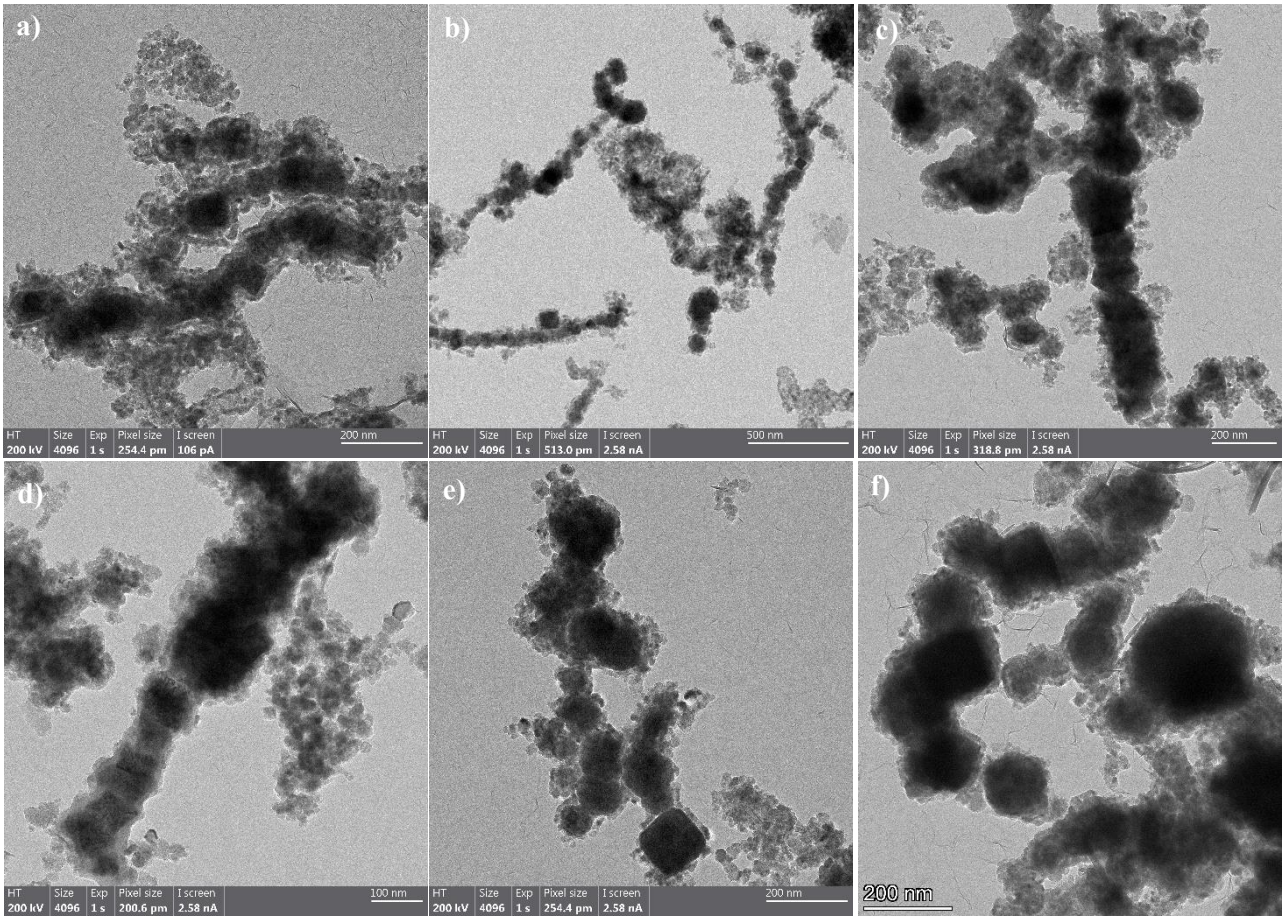

Figure S11. TEM images of 0.1S particle before reaction

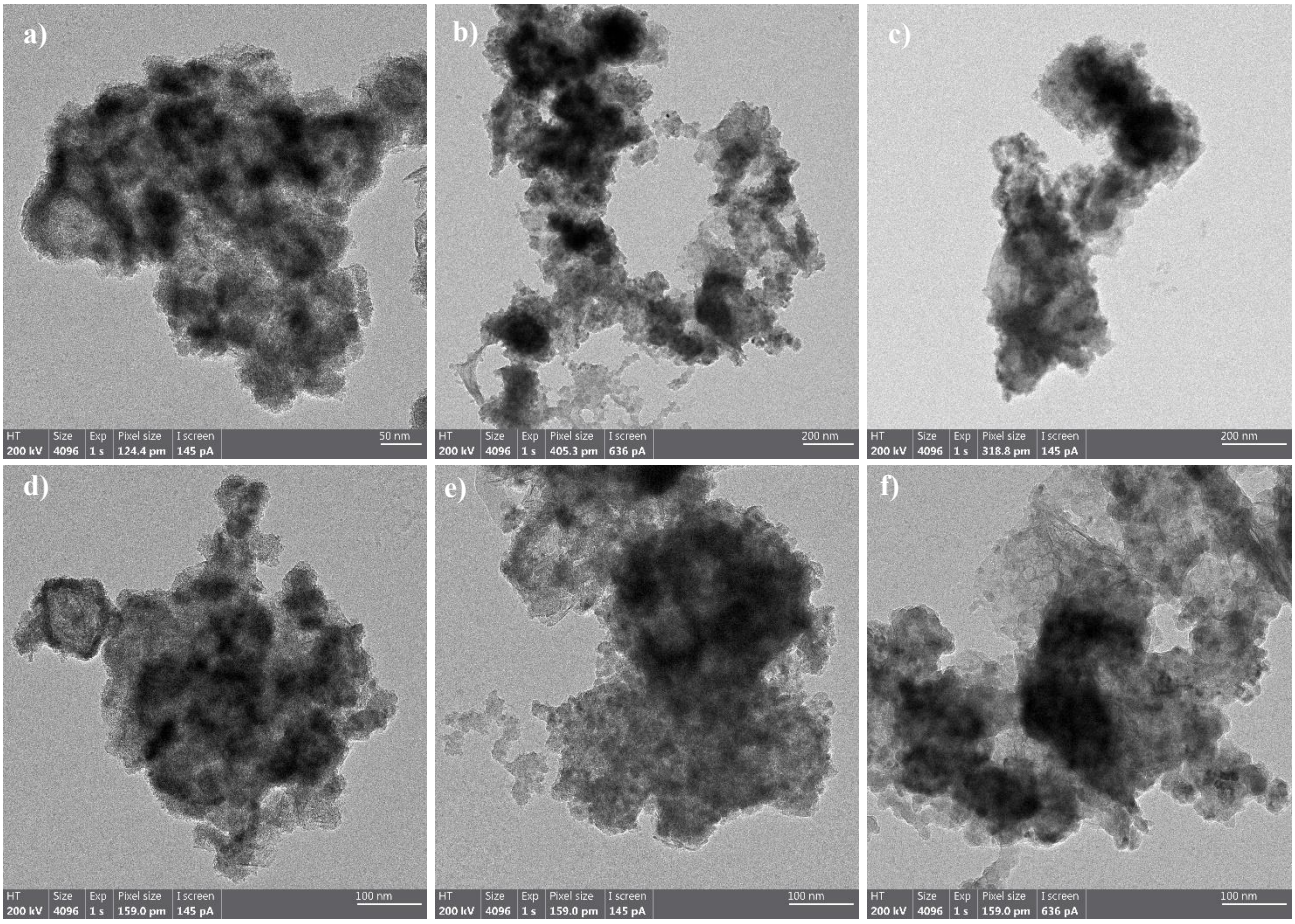

Figure S12. TEM images of 0.1S particle after reacting with phosphate and water for 1 hour

Reference

[1] Gillham, R. W., & O'Hannesin, S. F. (1994). Enhanced degradation of halogenated aliphatics by Zero-Valent iron. Ground Water, 32(6), 958–967.

[2] Scherer, M. M., Balko, B. A., Gallagher, D., & Tratnyek, P. G. (1998). Correlation analysis of rate constants for dechlorination by Zero-Valent iron. Environmental Science & Technology, 32(19), 3026–3033.

[3] O'Carroll, D. M., Sleep, B. E., Król, M., Boparai, H. K., & Kocur, C. M. (2013). Nanoscale zero valent iron and bimetallic particles for contaminated site remediation. Advances in Water Resources, 51, 104–122.

[4] Fu, F., Dionysiou, D. D., & Hong, L. (2014). The use of zero-valent iron for groundwater remediation and wastewater treatment: A review. Journal of Hazardous Materials, 267, 194–205.

[5] Lowry, G. V., & Johnson, K. M. (2004). Congener-Specific dechlorination of dissolved PCBs by microscale and nanoscale zerovalent iron in a Water/Methanol solution. Environmental Science & Technology, 38(19), 5208–5216.

[6] Mukherjee, R., Kumar, R., Sinha, A., Lama, Y., & Saha, A. K. (2015). A review on synthesis, characterization, and applications of nano zero valent iron (nZVI) for environmental remediation. Critical Reviews in Environmental Science and Technology, 46(5), 443–466.

[7] Ken, D. S., & Sinha, A. (2020). Recent developments in surface modification of nano zero-valent iron (nZVI): Remediation, toxicity and environmental impacts. Environmental Nanotechnology, Monitoring and Management, 14, 100344.

[8] Bhattacharjee, S., & Ghoshal, S. (2018c). Optimal design of sulfidated nanoscale zerovalent iron for enhanced trichloroethene degradation. Environmental Science & Technology, 52(19), 11078–11086.

[9] Xu, J., Avellan, A., Li, H., Liu, X., Noël, V., Lou, Z., Wu, Y., Kaegi, R., Henkelman, G., & Lowry, G. V. (2020b). Sulfur loading and speciation control the hydrophobicity, electron transfer, reactivity, and selectivity of sulfidized nanoscale zerovalent iron. Advanced Materials, 32(17), 1906910.

[10] Kim, E., Kim, J., Azad, A., & Chang, Y. S. (2011b). Facile synthesis and characterization of FE/FES nanoparticles for environmental applications. ACS Applied Materials & Interfaces, 3(5), 1457–1462.

[11] Han, Y., & Yan, W. (2016c). Reductive Dechlorination of Trichloroethene by Zero-valent Iron Nanoparticles: Reactivity Enhancement through Sulfidation Treatment. Environmental Science & Technology, 50(23), 12992–13001.

[12] Li, T., & Farrell, J. (2001c). Electrochemical Investigation of the Rate-Limiting Mechanisms for trichloroethylene and carbon tetrachloride reduction at iron surfaces. Environmental Science & Technology, 35(17), 3560–3565.

[13] Lymar, S. V., & Schwarz, H. A. (2012). Hydrogen Atom Reactivity toward Aqueous tert-Butyl Alcohol. Journal of Physical Chemistry A, 116(5), 1383–1389.

[14] Wojnárovits, L., Takács, E., Dajka, K., Emmi, S. S., Russo, M., & D'Angelantonio, M. (2004). Re-evaluation of the rate constant for the H atom reaction with tert-butanol in aqueous solution. Radiation Physics and Chemistry, 69(3), 217–219.

[15] Lou, Z., Zhou, J., Sun, M., Xu, J., Yang, K., Lv, D., Zhao, Y., & Xu, X. (2018). MnO2 enhances electrocatalytic hydrodechlorination by Pd/Ni foam electrodes and reduces Pd needs. Chemical Engineering Journal, 352, 549–557.

[16] Li, T., Li, X., Teng, Y., Wang, H., & Sun, H. (2023). Phosphidation of microscale zero-valent iron (P-mZVI) for enhanced dechlorination of trichloroethylene. Journal of Cleaner Production, 386, 135803.

[17] Gu, Y., Wang, B., He, F., Bradley, M. J., & Tratnyek, P. G. (2017). Mechanochemically sulfidated microscale zero valent iron: Pathways, kinetics, mechanism, and efficiency of trichloroethylene dechlorination. Environmental Science & Technology, 51(21), 12653–12662.

[18] Jin, X., Chen, H., Yang, Q., Hu, Y., & Yang, Z.. (2018). Dechlorination of carbon tetrachloride by Sulfide-Modified nanoscale zerovalent iron. Environmental Engineering Science, 35(6), 560–567.

[19] Xu, J., Avellan, A., Li, H., Clark, E. A., Henkelman, G., Kaegi, R., & Lowry, G. V. (2020b). Iron and sulfur precursors affect crystalline structure, speciation, and reactivity of sulfidized nanoscale zerovalent iron. Environmental Science & Technology, 54(20), 13294–13303.

[20] Zhang, Y., Ozcer, P. O., & Ghoshal, S. (2021b). A comprehensive assessment of the degradation of C1 and C2 chlorinated hydrocarbons by sulfidated nanoscale zerovalent iron. Water Research, 201, 117328.

[21] Li, T., Gao, C., Wang, W., Teng, Y., Li, X., & Wang, H. (2022). Strong influence of degree of substitution on carboxymethyl cellulose stabilized sulfidated nanoscale zero-valent iron. Journal of Hazardous Materials, 425, 128057.

[22] Ferry, J. L., & Glaze, W. H. (1998). Photocatalytic Reduction of Nitroorganics over Illuminated Titanium Dioxide: Electron Transfer between Excited-State TiO2 and Nitroaromatics. Journal of Physical Chemistry B, 102(12), 2239–2244.

[23] Johnson, T. W., Fish, W., Gorby, Y. A., & Tratnyek, P. G. (1998). Degradation of carbon tetrachloride by iron metal: Complexation effects on the oxide surface. Journal of Contaminant Hydrology, 29(4), 379–398.

[24] Xie, Y., & Cwiertny, D. M. (2013b). Chlorinated Solvent Transformation by Palladized Zerovalent Iron: Mechanistic Insights from Reductant Loading Studies and Solvent Kinetic Isotope Effects. Environmental Science & Technology, 47(14), 7940–7948.

[25] Mangayayam, M. C., Dideriksen, K., Ceccato, M., & Tobler, D. J. (2019b). The structure of sulfidized Zero-Valent iron by One-Pot Synthesis: Impact on contaminant selectivity and Long-Term performance. Environmental Science & Technology, 53(8), 4389–4396.

[26] Arnold, W. A., & Roberts, A. L. (2000). Pathways and Kinetics of Chlorinated Ethylene and Chlorinated Acetylene Reaction with Fe(0) Particles. Environmental Science & Technology, 34(9), 1794–1805.

[27] Marcus, P., Maurice, V., & Strehblow, H. (2008). Localized corrosion (pitting): A model of passivity breakdown including the role of the oxide layer nanostructure. Corrosion Science, 50(9), 2698–2704.

[28] Deshmukh, S. Saraph, R. Mehendale, Deshmukh, S. (2014). Novel hybrid exchanger for phosphate removal from water and wastewater. Jr. of Industrial Pollution Control 30(1) Pp 67-72.

[29] Gu, Y., Gong, L., Qi, J., Cai, S., Tu, W., & He, F. (2019). Sulfidation mitigates the passivation of zero valent iron at alkaline pHs: Experimental evidences and mechanism. Water Research, 159, 233–241.

[30] Rajajayavel, S. R. C., & Ghoshal, S. (2015b). Enhanced reductive dechlorination of trichloroethylene by sulfidated nanoscale zerovalent iron. Water Research, 78, 144–153.

[31] He, F., Li, Z., Shi, S., Xu, W., Sheng, H., Gu, Y., Jiang, Y., & Xi, B. (2018). Dechlorination of excess trichloroethene by bimetallic and sulfidated nanoscale Zero-Valent iron. Environmental Science & Technology, 52(15), 8627–8637.

[32] Cao, Z., Li, H., Lowry, G. V., Shi, X., Pan, X., Xu, X., Henkelman, G., & Xu, J. (2021c). Unveiling the Role of Sulfur in Rapid Defluorination of Florfenicol by Sulfidized Nanoscale Zero-Valent Iron in Water under Ambient Conditions. Environmental Science & Technology, 55(4), 2628–2638.

[33] Mangayayam, M. C., Alonso-De-Linaje, V., Dideriksen, K., & Tobler, D. J. (2020). Effects of common groundwater ions on the transformation and reactivity of sulfidized nanoscale zerovalent iron. Chemosphere, 249, 126137.

[34] Pinder, K. L. (1987b). Fogler, H. S. “elements of chemical reaction engineering”, prentice-hall, englewood cliffs, New Jersey 07632, 1986, 769 pages. Price $74.15 Canadian. Canadian Journal of Chemical Engineering, 65(3), 526–527.

[35] Siyuan, M. (2021). Degradation of chlorinated hydrocarbon contaminants by sulfidated nanoscale zerovalent iron: impact of particle sulfidation extent [Master's thesis, McGill University]

[36] Theurich, J., Lindner, A. M., & Bahnemann, D. W. (1996). Photocatalytic degradation of 4-Chlorophenol in aerated aqueous titanium dioxide suspensions: a kinetic and mechanistic study. Langmuir, 12(26), 6368–6376.

[37] Gaspar, D. J., Lea, A. S., Engelhard, M. H., Baer, D. R., Miehr, R., & Tratnyek, P. G. (2002). Evidence for Localization of Reaction upon Reduction of Carbon Tetrachloride by Granular Iron. Langmuir, 18(20), 7688–7693.

[38] Matheson, L. J., & Tratnyek, P. G. (1994). Reductive dehalogenation of chlorinated methanes by iron metal. Environmental Science & Technology, 28(12), 2045–2053.

Chapter 4. Overall Conclusions and Discussion

4.1 Major Conclusions

This thesis focuses on exploring the mechanisms behind the enhanced dechlorination capacity resulting from sulfidation of nZVI. In Chapter 1, a literature review is presented describing the different mechanisms that have been proposed for increased reactivity upon sulfidation of nZVI. Some even contradict with each other. Nevertheless, most discussions suggest the involvement of atomic hydrogen, which provides the most rational explanation on the boosted reactivity. In response to this, the Solvent Kinetic Isotope Effect (SKIE) methodology, that has been successfully applied to test involvement of atomic hydrogen is introduced in Chapter 2. By switching the solvent from H_2O to D_2O, any process involving atomic hydrogen as an intermediate would be greatly slowed while direct electron transfer is not affected. A matrix of batch experiments was conducted and the SKIE ratios (a ratio between rate constant values in H_2O and D_2O) turn out to be very low, indicating insignificant role of atomic hydrogen in the degradation of the target chlorinated organic compounds. Further attempts on assessing the formation of atomic hydrogen by S-nZVI was made by measuring its hydrogen uptake ability. Pd-nZVI, which is able to form atomic hydrogen following uptake of hydrogen gas, however with S-nZVI there is no uptake of hydrogen gas, which would suggest that atomic hydrogen is not formed. Among all existing techniques, Electron spin resonance (EPR) spectroscopy is the most direct evidence to prove existence of atomic hydrogen. Nickel is a prominent alternative to palladium for their similar catalytic functions in hydrogenation/dehydrogenation and a clear atomic hydrogen EPR signal was found on Ni-nZVI[1]. However, none of the studies with S-nZVI reported the detection of atomic hydrogen signal, with particle only, so far and only ·OH and

$SO4\cdot^-$ radical signals could be found in persulfate oxidation system[2-3]. So, in conclusion, there is very limited evidence showing the presence of atomic hydrogen when S-nZVI is degrading trichloroethylene (TCE) and carbon tetrachloride (CT). It is not a matter of pollutant type, but the ability for S-nZVI to produce atomic hydrogen is poor. Pd-nZVI and Ni-nZVI are very well-known bi-metallic nZVI particles that can form atomic hydrogen, and the mechanism of pollutant degradation by Ni-nZVI and Pd-nZVI usually undergoes hydrogenolysis[6]. In contrast, the S-nZVI degrades pollutant in β-elimination[7].

To explore the real mechanism, additional experiments were performed, which is described in Chapter 3. A previous study[4] demonstrated full inhibition of CT degradation with ZVI by just adding some amount of borate, but such an inhibitory effect is negligible for TCE degradation with S-nZVI with phosphate, an anion with similar properties to borate[5]. This disparity was further investigated by carrying out a matrix of experiments with two pollutants (i.e., TCE and CT) and particles with three sulfur doses (i.e., 0, 0.01, 0.1), an alternate reaction mechanism was proposed to interpret results. Briefly, this is described as direct electron transfer at iron (hydr)oxides sites contribute to high reactivity to contaminants such as CT, whereas electron transfer at FeS sites contribute to high reactivity to TCE. The results suggest that morphological changes arising from particle localized breakdown (pitting) also contribute to the formation of new reactive sites which result in high particle reactivity. Moreover, inter-species competition experiments were conducted to verify the proposed mechanism, and which further advances the hypothesis for a change in the rate determining step of pollutant degradation on different sites. Finally, intra-species competition experiments were carried out and the results were fitted by Langmuir–Hinshelwood–Hougen–Watson (LHHW) model to examine the rate determining step.

The fitting clearly supports the existence of different sites during degradation that possess different properties.

4.2 Limitations

The most meaningful contribution of this work is it is the first time to introduce phosphate to block certain sites of S-nZVI. Also, it is also the first report of concentration correlation on degradation rate constant. By altering the concentration and fitting the result based on LHHW model, different sites can be distinguished easily. However, just like all other proposed mechanisms, it has some limitations.

First, the addition of phosphate brings one more variable to the system. Iron phosphate, an undesired precipitation product formed when electron is transferred from particle to pollutant, may either adsorb organic pollutants, or form a new active site. This creates uncertainty on the relevance of the proposed mechanism for degradation of other organic chlorinated compounds with S-nZVI. For pollutants that can be easily degraded or adsorbed on iron phosphate site, the result would be confusing.

The other drawback of the study is the use of LHHW model. One important assumption made by this model is that the total number of active sites should be constant before and after the reaction. However, based on the result from CT degradation by S-nZVI, it is obvious that an increase in active site would take place. That's why the fitting result have a large standard deviation value. There is no easy way to address this except ensuring the reaction time is short enough that the conversion of primary product into secondary product is limited, like acetylene to ethene for TCE degradation by S-nZVI. In this way, the product would not compete electrons with target pollutant.

Reference

[1] Tian, F., Tang, J., Zeng, J., Luo, Z., Zhang, L., Tang, F., Han, Z., & Yang, X. (2022). Degradation of atrazine by Ni-doped sulfidated microscale zero-valent iron: Mechanistic insights for enhanced reactivity and selectivity. Chemical Engineering Journal, 435, 135120.

[2] Chen, J., Luo, H., Luo, D., Chen, Y., Tang, J., Ma, H., & Pu, S. (2023). New insights into the degradation of nitrobenzene by activated persulfate with sulfidated nanoscale zero-valent iron: synergistic effects of catalyst reduction and reactive oxygen species oxidation. Separation and Purification Technology, 322, 124252.

[3] Xiong, Y., Zhou, T., Bao, J. et al. Degradation mechanism of Bisphenol S via hydrogen peroxide/persulfate activated by sulfidated nanoscale zero valent iron. Environ Sci Pollut Res 30, 83545–83557 (2023).

[4] Johnson, T. W., Fish, W., Gorby, Y. A., & Tratnyek, P. G. (1998b). Degradation of carbon tetrachloride by iron metal: Complexation effects on the oxide surface. Journal of Contaminant Hydrology, 29(4), 379–398.

[5] Mangayayam, M. C., Alonso-De-Linaje, V., Dideriksen, K., & Tobler, D. J. (2020b). Effects of common groundwater ions on the transformation and reactivity of sulfidized nanoscale zerovalent iron. Chemosphere, 249, 126137.

[6] He, F., Li, Z., Shi, S., Xu, W., Sheng, H., Gu, Y., Jiang, Y., & Xi, B. (2018b). Dechlorination of excess trichloroethene by bimetallic and sulfidated nanoscale Zero-Valent iron. Environmental Science & Technology, 52(15), 8627–8637.

[7] Zhang, Y., Ozcer, P. O., & Ghoshal, S. (2021c). A comprehensive assessment of the degradation of C1 and C2 chlorinated hydrocarbons by sulfidated nanoscale zerovalent iron. Water Research, 201, 117328.